



Importance of aerosol composition and mixing state for cloud droplet activation over the Arctic pack ice in summer

C. Leck and E. Svensson

Department of Meteorology and Bert Bolin Centre for Climate Research, Stockholm University, 10691 Stockholm, Sweden

Correspondence to: C. Leck (lina@misu.su.se)

Received: 15 April 2014 – Published in Atmos. Chem. Phys. Discuss.: 19 August 2014

Revised: 8 January 2015 – Accepted: 6 February 2015 – Published: 6 March 2015

Abstract. Concentrations of cloud condensation nuclei (CCN) were measured throughout an expedition by ice-breaker around the central Arctic Ocean, including a 3 week ice drift operation at 87° N, from 3 August to 9 September 2008. In agreement with previous observations in the area and season, median daily CCN concentrations at 0.2 % water vapour supersaturation (SS) were typically in the range of 15 to 30 cm⁻³, but concentrations varied by 2 to 3 orders of magnitude over the expedition and were occasionally below 1 cm⁻³. The CCN concentrations were highest near the ice edge and fell by a factor of 3 in the first 48 h of transport from the open sea into the pack ice region. For longer transport times they increased again, indicating a local source over the pack ice, suggested to be polymer gels, via drops injected into the air by bubbles bursting on open leads. We inferred the properties of the unexplained non-water soluble aerosol fraction that was necessary for reproducing the observed concentrations of CCN. This was made possible by assuming Köhler theory and simulating the cloud nucleation process using a Lagrangian adiabatic air parcel model that solves the kinetic formulation for condensation of water on size resolved aerosol particles. We propose that the portion of the internally/externally mixed water insoluble particles was larger in the corresponding smaller aerosol size ranges. These particles were physically and chemically behaving as polymer gels: the interaction of the hydrophilic and hydrophobic entities on the structures of polymer gels during cloud droplet activation would at first only show a partial wetting character and only weak hygroscopic growth. Given time, a high CCN activation efficiency is achieved, which is promoted by the hydrophilicity or surface-active properties of the gels. Thus the result in this study argues that the behaviour of the high Arctic aerosol in CCN-counters operating

at water vapour SSs >0.4 % (high relative humidities) may not be properly explained by conventional Köhler theory.

1 Introduction

Twomey (1974) showed that the state of division of the available water in clouds determines the amount of short wave radiation scattered back to space, the effect being largest in optically thin clouds with few water drops. This is particular true for Arctic low-level clouds (Walsh et al., 2002; Tjernström et al., 2008). Furthermore, these Arctic low-level clouds, while controlling the surface radiation balance, have a pronounced influence on the melting and freezing of the perennial sea ice (Intrieri, 2002; Kay and Gettelman, 2009; Mauritsen et al., 2010; Sedlar et al., 2011). For most of the year, such clouds tend to warm the surface, but during the peak melt season at the end of the summer, low-level clouds could cool the ice surface and thereby influence the timing of the autumn freeze-up. Earlier freeze-up will cause thicker ice that might melt less during the following summer, surviving into the subsequent winter. If such a process were to recur over several years, it could delay or even prevent sea ice from melting completely during the Arctic summer. In other words, it would constitute a negative feedback. The concentration of cloud water drops is largely determined by the concentration of nuclei on which cloud drops can form (cloud condensation nuclei, CCN). This also requires that the meteorological conditions – wind, humidity and temperature – are favourable. Measurements of cloud condensation number concentrations (CCNC) over the pack ice are scarce due to the remoteness of the area. Apart from research carried out in a series of four international ice-breaker expedi-

tions to the high Arctic in the summers of 1991 (Leck et al., 1996), 1996 (Leck et al., 2001) and 2001 (Leck et al., 2004; Tjernström et al., 2004) and in 2008 (Tjernström et al., 2014) there has been no effort relevant to the formation of low-level clouds, north of 80°, during conditions when influences from man-made particle sources were limited. CCNC have been observed to vary by 3 orders of magnitude over the period July to September and commonly by an order of magnitude within a day, but were usually lower than 100 cm^{-3} , occasionally less than 1 cm^{-3} (Lanefors et al., 1983; Bigg et al., 1996, 2001; Bigg and Leck, 2001a; Leck et al., 2002; Mauritsen et al., 2011). Figure 6 in Mauritsen et al. displays frequency distributions of observed CCNC from all four expeditions measured at different water vapour supersaturations (SS), ranging from 0.1 to 0.8%. All four populations showed an overall consistent distribution, with three-quarters of the CCNC being greater than 10 but less than about 100 cm^{-3} , and medians typically in the range 15 to 50 cm^{-3} as reported by Bigg et al. (1996) and Bigg and Leck (2001a).

In searching for a relationship between the properties of the summer high Arctic aerosol and its ability to form CCN, Zhou et al. (2001) calculated CCNC by assuming equilibrium Köhler theory (Köhler, 1936). The calculations used aerosol number size distribution data and additional hygroscopic growth information and assumed that the calculated CCN particles were composed of ammonium sulfate, sodium chloride and a nearly water-insoluble fraction. The closure study resulted in an over-prediction of the calculated CCNC (more CCN were calculated than measured) of around 30%. In a separate study on the same CCN data Bigg and Leck (2001a) made the simpler assumption that all particles in the number size distribution were composed of pure ammonium sulfate. A similar over-prediction resulted, as reported by Zhou et al. (2001). Sorting the CCN data according to meteorological conditions combined with added information on particle morphology and state of mixture, Leck et al. (2002) concluded that other components, probably organics, depressed the nucleating ability of the particles. However, on clear-sky days, there were a majority of occasions on which observed CCNC were higher than predicted from a sulfate composition and the measured size distribution. Since equilibrium Köhler theory cannot take kinetic effects into account, which can cause erroneous results when considering the competition of aerosol particles of different size for water vapour, the cloud nucleation process was in addition simulated with a Lagrangian parcel model (Lohmann and Leck, 2005). In order to explain the observed CCNC over the pack ice the authors found it necessary to invoke an Aitken mode composed of highly surface-active organics, externally mixed with a sulfur-containing population. Most recently Martin et al. (2011) performed yet another CCN closure study that was representative for high Arctic summer conditions. To predict the CCNC, the closure was based on data on average measured from 0.1 to 0.7% water vapour SS and κ -Köhler theory (Petters and Kreidenweis, 2007).

This approach differed from the previous studies, which used only one level of water vapour SS (0.2%) in the comparison between measured and modelled CCNC. Further, Martin et al. (2011) used highly time resolved (average over 5 min) sub-micrometre aerosol bulk chemical compositions (sulfate, nitrate, organics and methane sulfonate) obtained by an aerosol mass spectrometer; see Chang et al. (2011) for details. The authors derived total hygroscopicity parameters by permuting parameter values for the components and the solubility of the organics. The surface tension was assumed to be constant and equal to that of pure water. Consistent with the previous results of Zhou et al. (2001) and Bigg and Leck (2001a), the calculations generally tended to over-predict the observed CCNC, with about 30–60% for water vapour SS above 0.4%. To explain the results the authors proposed that the portion of the particles assumed to be made up by internally mixed water insoluble organics was larger for the smaller size ranges. The opposing CCN-closure results discussed above indicate that the observed presence of organic constituents, possibly both marine primary and secondary, most likely will play an important role in determining the ability of the aerosol collected over the Arctic pack ice area to act as CCN.

This study will attempt to further reduce some of the uncertainties surrounding the CCN properties promoting/suppressing cloud droplet formation over the Arctic pack ice area with limited influences from man-made activities. This will be made possible by using observed sensitivity (on average between 0.1 and 0.7% water vapour SS) of measured CCNC combined with Köhler theory and by simulating the cloud nucleation process using a Lagrangian adiabatic air parcel model that solves the kinetic formulation for condensation of water on size resolved aerosol particles. The simulations will be based on the diffusional growth equation as was used in Lohmann and Leck (2005). The CCNC will be predicted from observed aerosol number size distribution data and additional hygroscopic growth information, and by assuming that the calculated CCN particles were composed of an inorganic/organic aerosol system. In the latter case we will use the determined aerosol bulk chemistry obtained from highly size resolved impactor samples to show the extent to which determined water-soluble dimethyl sulfide (DMS) oxidation products, sodium chloride and other inorganic compounds contributed to the CCN population. As a surrogate for the unexplained fraction assumed to be organic in nature we will use various water soluble, slightly water soluble and non-water soluble proxy constituents. The simulated CCNC will be compared to the observed CCNC at water vapour SS on average ranging between 0.1 and 0.7%, collected during the Arctic Summer Cloud Ocean Study (ASCOS)¹ on board

¹The interdisciplinary programme of ASCOS was conducted in the fields of marine biology and chemistry, atmospheric chemistry, oceanography and meteorology with the overall aim to improve our understanding of low-level cloud formation and possible climate

the Swedish icebreaker *Oden* in 2008 in the open waters and marginal ice zone of the Greenland Sea–Fram Strait area and over the pack ice north of 80°. For detailed information on the quality and data processing of the measurements of CCN, aerosol number size distributions and aerosol hygroscopic growth we refer to Martin et al. (2011), Heintzenberg and Leck (2012) and Zhou et al. (2001).

2 Route of the expedition and measuring systems and methods

2.1 Route and platform

The CCNC simulations presented here utilize measurements carried out on board the icebreaker *Oden* as part of ASCOS. Samples were collected in surface air over the central Arctic Ocean during the biologically most active summer period. The expedition departed from Longyearbyen, Svalbard, on 2 August 2008 (day of year (DOY) 215; note the leap year) and headed north for the pack ice of the central Arctic Ocean. There was a transition from the “marginal ice zone” having 20–70 % ice cover and the “pack ice region” having 80–95 % ice cover. On 12 August (DOY 225) *Oden* was anchored to a large ice floe, slightly north of 87° N, and proceeded to drift with it for the following 3 weeks (referred to as the pack ice (PI) drift), until midnight between 1 and 2 September (DOY 245–246). In transit to the ice drift, additional stations were set up at the ice edge and an open water station in the Greenland Sea–Fram Strait area: an open water station (OW-1) on 3 August 2008 (DOY 216–216.5) (78.2° N; 7.5° E) followed by a station in the marginal ice zone (MIZ-1) starting on 4 August 2008 (DOY 217.5) (79.9° N; 6.1° E). On the way back from the ice drift, a second marginal ice edge station (MIZ-2) was set up at the ice edge on 6 September immediately followed by a final open water station (OW-2) ending on 7 September in the Greenland Sea. As several of the instruments were not in use, no data from the MIZ2 and OW2 stations are discussed in this study. *Oden* arrived back at Longyearbyen on 9 September (DOY 253). A map of the route with the ice drift magnified is shown in Fig. 1. All times are reported in universal time coordinate (UTC). The sun was continuously above the horizon of the expedition.

2.2 Particle measurement systems

The measurements utilized in this study were made from a sampling manifold with an impactor (Anderson Inc., Atlanta, GA) 50 % cutoff diameter of 10 µm (PM₁₀) at 25 m height on board *Oden*. The PM₁₀ inlet was identical to the one used during all three previous expeditions in the summers of 1991, 1996 and 2001. Direct contamination from the ship was excluded by using a pollution controller, turning off all

feedback processes over the central Arctic Ocean. Tjernström et al. (2014) give more details.

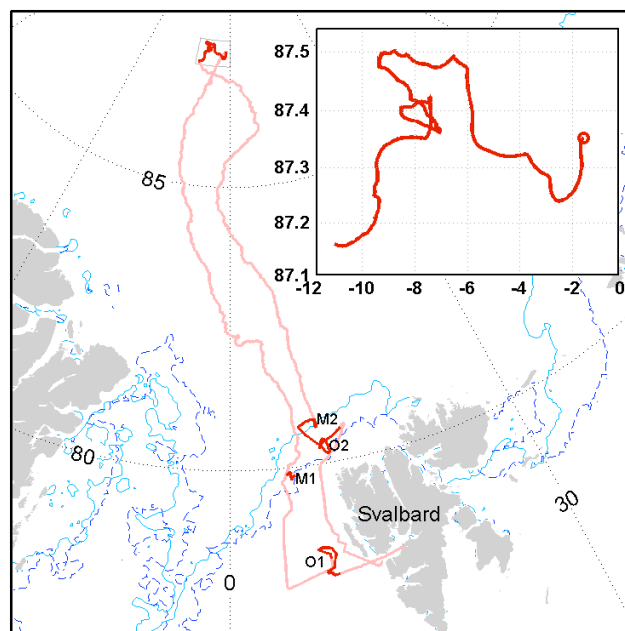


Figure 1. Map of the ASCOS cruise track (pink) with ice-drift period (PI-drift) highlighted (red) and (inset) shown in detail with the start of the drift marked by the circle. The left-hand part of the track shows the initial northward track while the right-hand part shows the southward, return track. Convoluted track lines in open water, OW (O1 and O2) and at the ice edge, MIZ (M1 and M2) are associated with shorter sampling stations. The light blue line illustrates the ice edge at the time of entry and the darker blue line at the time of exit.

the pumps of the samplers, in direct connection to the sampling manifold. To maximize sampling time safe from pollution our strategy was to keep the sampling manifold facing upwind to avoid sampling of ship exhausts. This necessitated a “harbour” in the ice in which the ship, with its non-rotating mast on the fourth deck, could be moored in several different directions and turned as the wind direction changed. Further details of the location and properties of air intakes and instruments, position on the ship, pumping arrangements and precautions to exclude contaminated periods can be found in Leck et al. (2001) and Tjernström et al. (2014). Key instruments used and important measurement details are discussed below.

1. Aerosol particles that are active as CCN were measured continuously using two identical CCN counters (Roberts and Nenes, 2005) operating in parallel. Aerosol particles enter the CCN counter through an inlet at the top and pass through a cylindrical column where they can activate and grow to droplet size. In the column a temperature gradient is established, with the lowest temperature at the top. The walls of this column are wetted with water. Thus, heat and water vapour are transported towards the centre of the column by dif-

fusion. As heat diffuses more slowly than water in air in the temperature range used, a constant water vapour SS is established in the centre of the column. This SS can be adjusted by changing the temperature gradient of the column. At the outlet of the column the activated particles are counted with an optical particle counter (OPC) and collected in bins of different sizes. The CCN counter defines a CCN as a particle having a wet diameter $> 1 \mu\text{m}$ and a positive growth rate. The CCN counter undercounts particles if they have not grown larger than $1 \mu\text{m}$ by the time they reach the OPC.

The first CCN counter was set to a constant water vapour SS of ca. 0.2 % averaged over 1 minute, which was slightly increased later for better comparison with CCN data collected during the three former expeditions: measurements were performed at 0.17 % SS between 3 August (DOY 216) and 15 August (DOY 228) and at 0.21 % SS for the remaining period, 16 August (DOY 229) to 9 September (DOY 253). The second counter scanned five different water vapour SSs, on average ranging between 0.1 and 0.7 %. After each calibration the settings of the second counter were adjusted. Therefore, the water vapour SS at which the CCNC were measured varies for different time periods, with a measurement period of 30 min each. The average values in percent are given in *italic* and the spread in brackets: *0.10* (0.082–0.106), *0.15* (0.126–0.161), *0.20* (0.171–0.233), *0.41* (0.347–0.521), *0.73* (0.613–0.952). This enabled a determination of the sensitivity of measured CCN to the choice of water vapour SS. Martin et al. (2011) give more information on the quality and data processing of the CCNC measurements.

2. Aerosol particle number size distributions at 10 to 20 min time resolution were measured in 45 bins from 3 to 800 nm in diameter using a twin differential mobility particle sizer (TDMPS; Birmilli et al., 1999). Throughout this paper all number particle sizes will be referred to as dry geometric mean diameters (GMDs). In the discussion to follow we will refer to the following modal GMD representation of the observations: the Aitken mode (25–70 nm), the accumulation mode (70–1000 nm) and the recently nucleated mode (< 10 nm). Table 1 shows examples of the particle number variability seen by the TDMPS during the duration of the impactors. Tabulated are the 25th, 50th (median) and 75th percentile aerosol number concentrations for 40, 80 and 300 nm diameters, respectively. Further details on the quality and data processing of these measurements are available in Heintzenberg and Leck (2012).
3. To measure the growth of individual particles in diameter sizes of 31, 50, 72, 108, 163 and 263 nm from the dry state (< 20 % RH) to a set RH, a hygroscopic tan-

dem differential mobility analyser (H-TDMA) instrument was used. Zhou et al. (2001) gives details.

4. Aerosol bulk chemical composition was determined from a 13-stage ($30 \text{ dm}^3 \text{ min}^{-1}$) LPI (Dekati, <http://dekati.com>) impactor. Upstream of the impactor, the temperature and the RH (on average 40 %) of the incoming sample air were measured and recorded using mini probes and a data acquisition system custom made for the expedition by Vaisala. The LPI impactor had 50 % cut-off diameters of: 10.0, 6.57, 3.96, 2.45, 1.60, 0.990, 0.634, 0.391, 0.253, 0.165, 0.104, 0.060 and $0.029 \mu\text{m}$ equivalent aerodynamic diameter (EAD). Polycarbonate collection foils were used as the collection substrate. The impaction stages 1 (10.0–6.57 μm EAD), 2 (6.57–3.96 μm EAD) and 3 (3.96–2.45 μm EAD) at the inlet of the impactor were coated with grease (Apiezon-L dissolved in hexane) to prevent the bounce-off of larger particles with their relatively large masses onto the downstream stages. The amount of mass, if any, bounced from upper stages is difficult to quantify. However, the fact that sodium concentration in the submicron stages did not systematically follow the supermicron sodium concentration is an indirect indication that the substrate greasing was sufficient to reduce or eliminate serious bounce-off. Blank levels were determined by loading six impactors with the substrates at the sampling site for the length of the sampling period but with no air drawn through it. The detailed size segregated LPI impactor required relatively long sampling times of 20–40 h resulting in 18 sampling periods obtained during the course of ASCOS.

2.3 Water soluble mass determination

To allow for subsequent chemical determinations all substrates, ambient samples and blanks were carefully handled in a glove box (free from particles, sulfur dioxide and ammonia) both prior to and after sampling. At the time of the chemical analyses, still in the glove box, the substrates were extracted (in centrifuge tubes) with 5 cm^3 deionized water (Millipore Alpha-Q, conductivity $18 \text{ M}\Omega \text{ cm}$). For sufficient extraction the substrate extracts were finally placed in an ultrasonic bath for 60 min. The extracts were then analysed for major cations, anions and weak anions by chemically suppressed ion chromatography (IC, Dionex ICS-2000). The anions were analysed with Dionex AG11/AS11 columns and the cations with CG16/CS16. A Dionex ATC-1 column was used before the injection valve to trap carbonates and other ionic contaminants. The injection volume was $50 \mu\text{dm}^3$. Quality checks of the IC-analyses were performed with both internal and external reference samples (organized by EANET, 2008). Systematic errors were less than 2 % (with the exception of magnesium, Mg^{2+} , with less than 3 %) for all ionic components. The analytical detection limits obtained for the various ions, defined as twice the

level of peak-to-peak instrument noise, were 0.20, 0.05, 0.01, 0.01, 0.01, 0.05, 0.00, 0.00, 0.02 and 0.01 $\mu\text{eq dm}^{-3}$ for ammonium: NH_4^+ , sodium: Na^+ , potassium: K^+ , magnesium: Mg^{2+} , calcium: Ca^{2+} , chloride: Cl^- , MSA: CH_3SOO^- , oxalate: $\text{C}_2\text{O}_4^{2-}$, nitrate: NO_3^- and sulfate: SO_4^{2-} , respectively. The overall analytical accuracy was better than 3 % and 5 % for the anions and cations, respectively.

Blank levels were determined by loading 6 impactors with: 60 (6 impactors each, 10 stages) non-greased substrates and 18 (6 impactors each, 3 stages) greased substrates. The blank values for the non-greased impactors obtained for the various ions, defined as average and 1σ , were 0.20 ± 0.03 , 0.13 ± 0.02 , 0.02 ± 0.007 , 0.02 ± 0.005 , 0.12 ± 0.04 , 0.14 ± 0.02 , 0.00 ± 0.00 , 0.00 ± 0.00 , 0.06 ± 0.01 , $0.10 \pm 0.01 \mu\text{eq dm}^{-3}$ for NH_4^+ , Na^+ , K^+ , Mg^{2+} , Ca^{2+} , Cl^- , MSA, $\text{C}_2\text{O}_4^{2-}$, NO_3^- and SO_4^{2-} , respectively. The corresponding values for the greased substrates were 0.29 ± 0.03 , 0.80 ± 0.16 , 0.03 ± 0.004 , 0.08 ± 0.005 , 0.29 ± 0.04 , 0.22 ± 0.05 , 0.00 ± 0.00 , 0.00 ± 0.00 , 0.10 ± 0.01 and $0.13 \pm 0.03 \mu\text{eq dm}^{-3}$ for NH_4^+ , Na^+ , K^+ , Mg^{2+} , Ca^{2+} , Cl^- , MSA, $\text{C}_2\text{O}_4^{2-}$, NO_3^- and SO_4^{2-} , respectively.

During the expedition LPI levels (sample minus blank) of MSA, Cl^- , NO_3^- , SO_4^{2-} , oxalate, Na^+ , K^+ , Mg^{2+} and Ca^{2+} down to 0.002, 0.030, 0.009, 0.010, 0.007, 0.030, 0.004, 0.008 and $0.032 \text{ nmol m}^{-3}$, respectively, were detected.

2.4 Converting the aerosol chemical mass distributions to aerosol chemical number size distributions

The size resolved chemical mass concentration was converted to a chemical number size distribution by firstly transposing the LPI impactor 50 % cut-off diameters (EAD at 40 % RH) to dry (20 % RH) GMD. Following the assumptions made in Hinds (1999) and Tang and Munkelwitz (1994), the following dry GMDs resulted: 0.019–0.40 μm (bin-1), 0.40–0.71 μm (bin-2), 0.71–0.116 μm (bin-3), 0.116–0.181 μm (bin-4), 0.181–0.284 μm (bin-5), 0.284–0.466 μm (bin-6), 0.466–0.732 μm (bin-7), 0.732–1.19 μm (bin-8), 1.19–1.82 μm (bin-9), 1.82–2.95 μm (bin-10), 2.95–4.91 μm (bin-11), 4.91–7.59 μm (bin-12). A size-dependent particle density (on average 1.35 g cm^{-3}) was calculated assuming mixtures of mainly sea salt, ammonium sulfate and MSA with smaller amounts of oxalate, potassium, calcium, magnesium and water similar to those observed. From varying only the average density between 1.2 and 1.4 g cm^{-3} the uncertainty in the transposed EAD to GMD was estimated to be about $\pm 5\%$. To reduce the calculated GMD from 40 to 20 % RH an observed hygroscopic growth factor of 1.15 was used. If we assume a $\pm 10\%$ uncertainty in the observed hygroscopic growth factors and add the $\pm 5\%$ uncertainties from the density estimates, the overall uncertainty in the transposition from EAD at 40 % RH to dry GMD is $\pm 11\%$. Thereafter we interpolated the water soluble mass composition for each of the impactor bins (1–7) to the TDMPS bins within the 20 to

800 nm diameter size range. The mass concentrations were then converted to number concentrations. Since the mass to number conversion depends on the cube of the diameter, the uncertainty of the values resulting from the conversion ranged between 70 and 140 %.

2.5 Air trajectories and time spent over the pack ice

The vertical structure of the atmosphere was typical for central Arctic summer during the expedition. The air layer closest to surface was shallow and well mixed with depths usually below 200 m. This layer was capped by a temperature inversion with a stable stratification of the atmosphere aloft due to the advection of warmer air from the south (Tjernström et al., 2012). The backward trajectories were calculated² for an arrival height in the well-mixed layer within the Arctic boundary layer, 100 m above surface level, at hourly intervals. The height of 100 m is a compromise to ensure that at least the receptor point is fairly close to the surface where the samples were collected (25 m above sea level), and at least in the well-mixed layer, but also that trajectories, due to rounding errors and interpolation, would not run too great a risk of “hitting the surface” in the backward trajectory calculations. Using *Oden*'s position as a starting point of the backward trajectory calculations gave a point that is very precisely measured with GPS. Backward trajectories have several sources of uncertainty, which generally grows with the length of the trajectory. Most uncertain is transport in the vicinity of strong gradients, such as frontal zones, while within a single air mass the trajectory calculations are likely to be more reliable.

With the help of the back-trajectories and ice maps³ the time elapsed since the air was last in contact with the open ocean was computed in the way that Nilsson (1996) reported. It will be referred to as day over ice (DOI). The calculated DOI thus marks the end point for an air parcel that left the ice edge between 0 and 10 days ago (resolved by the length of the trajectories). The measure of DOI will in the later analyses be used as a simple parameter to summarize the evolution of the aerosol as a function of the synoptic scale systems since their last contact with open sea. Calculated cumulative travel times over ice for ASCOS showed that most trajectories spent at least 3 days (median 3.3 days) over the pack ice before reaching *Oden*. Travel times less than 2 days were en-

²The NOAA HYSPLIT (Hybrid Single-Particle Lagrangian Integrated Trajectory) model (Draxler and Rolph, 2011; Rohph, 2011) was used to calculate three-dimensional 5 and 10 day backward trajectories of the air reaching *Oden*'s position. The trajectory calculations were based on data from the Global Data Assimilation System (GDAS) of the National Weather Service's National Center for Environmental Prediction (NCEP). Vertical motion in the trajectory runs was calculated using the model's vertical velocity fields.

³Ice maps from Satellite-sensor, AMSR-E, “level 1A” with the data sourced from NSIDC (Boulder), United States, finalized at Bremen University, <http://iup.physik.uni-bremen.de:8084/amsr/amsr.html> were used.

Table 1. The 25th, 50th (median) and 75th percentile aerosol number concentrations seen by the TDMS for 40, 80 and 300 nm diameter sizes separately for the impactor samples at the marginal ice zone (MIZ-1) and over the pack ice (PI-1, 8, 10, 13 and 15). Values are at STP. Also listed is the information on sampling start–stop times of the impactors.

Sample	Start time (UTC) DOY	End time (UTC) DOY	$N_{40\text{nm}}$			$N_{80\text{nm}}$			$N_{300\text{nm}}$		
			50th percentile cm^{-3}	25th percentile cm^{-3}	75th percentile cm^{-3}	50th percentile cm^{-3}	25th percentile cm^{-3}	75th percentile cm^{-3}	50th percentile cm^{-3}	25th percentile cm^{-3}	75th percentile cm^{-3}
MIZ-1	217.503	218.508	704	536	806	110	90	126	15	9.5	23
PI-1	225.967	227.321	49	31	121	32	10	63	3.3	1.3	7.3
PI-8	235.049	236.253	932	855	1094	190	144	216	1.4	0.39	5.1
PI-10	237.625	238.271	47	20	61	54	20	89	3.8	2.4	5.6
PI-15	244.826	245.977	0.90	0.55	2.2	0.97	0.25	2.8	0.60	0.02	1.8

countered around 30 % and travel times of 4 days and longer covered about 40 % of the cases.

3 Computational methods

Köhler (1936) describes the relationship between chemical properties, size and water vapour SS present at the surface of an aerosol droplet in thermodynamic equilibrium. The Köhler theory consists of the Kelvin effect, which describes the influence on water vapour SS pressure from the curvature of the spherical surface of an aerosol droplet, and the Raoult effect, which represents the influence from the solute. One key parameter in the Kelvin term is the surface tension. The surface tension of an aerosol particle is influenced not only by the curvature of the droplet but also by the concentration of amphiphilic solutes (Hede et al., 2011). Thus inorganic salts could be assumed to have an increasing effect on surface tension due to the ionic interactions, whereas surface-active organic compounds decrease the surface tension due to the amphiphilic properties disturbing the hydrogen bonding at the air–water interface. If a thermodynamic equilibrium with the environment of the aerosol droplet can be assumed, the droplet diameter size of a growing CCN particle can be calculated at a specific water vapour SS pressure. In the simplest use of the traditional Köhler theory keeping all parameters constant, the larger the aerosol droplet diameter is, the lower the critical water vapour SS pressure that is required for final activation into a cloud droplet.

The water vapour SS pressure over an aqueous aerosol droplet can also be expressed to depend on the droplet water activity (a_w) according to:

$$SS = a_w \exp(4\sigma_{s/a} M_w / RT \delta_w D), \quad (1)$$

where $\sigma_{s/a}$ is the surface tension between the solution and air, M_w is the molecular weight of the water solution, δ_w the density of the solution, R is the universal gas constant, T is the absolute temperature and D is the diameter of the droplet at the water vapour SS pressure. The droplet water activity, a_w , is a straightforward parameter, which can be measured directly in laboratory experiments. Svenningsson et al. (2006)

measured water activities as functions of solution molality for various mixtures of inorganic and organic compounds, and gave parameterizations. In this study we have used the MIXSEA mixture (ammonium sulfate 50, sodium chloride 30, succinic acid 10 and fulvic acid 10 %) parameterization.

Equation (1) can be reformulated using κ -Köhler theory (Petters and Kreidenweis, 2007). κ -Köhler theory is a one-parameter model, where the solute hygroscopicity parameter, κ , combined with the Kelvin term represents a measure of aerosol droplet water uptake and activity and thus determines the equilibrium water vapour SS over an aqueous droplet. Values of κ for specific constituents, or mixtures thereof, can be determined experimentally. Fitted values of κ for individual aerosol constituents may be combined to represent the hygroscopic behaviour of mixed aerosol particles of known composition. The water vapour SS pressure over an aqueous aerosol droplet could be expressed as:

$$SS = D^3 - D_d^3 / D^3 - D_d^3 (1 - \kappa) \exp(4\sigma_{s/a} M_w / RT \delta_w D), \quad (2)$$

where D_d is the volume equivalent diameter of the dry aerosol particle. κ depends on the water activity of the aerosol droplet and the volumes of the dry particle and of the aerosol droplet. It ranges between 0 for water-insoluble particles, and values > 1 for very water soluble salts ($\kappa = 1.28$ for NaCl). κ of an aerosol droplet is defined as the sum of the products of the κ values of all single solute components, i , in the aerosol droplet and their corresponding volume fractions $\epsilon_i = V_i / V_{\text{tot}}$, thus $\kappa_{\text{tot}} = \sum_i \kappa_i \epsilon_i$. To calculate κ_{tot} , κ values and densities for the separate mass constituents measured by the impactors had to be assumed. As with traditional Köhler theory, the maximum in water vapour SS computed for a specified initial dry particle size (referred to as the activation limit dry diameter) and composition (expressed by κ) determines the particle's critical water vapour SS (SSc) for activation to a cloud droplet.

Since equilibrium Köhler theory cannot take kinetic effects into account, and this can cause erroneous results when considering the competition of aerosol particles of different size for water vapour, we simulated the cloud nucleation process by assuming Köhler theory combined with a Lagrangian

adiabatic air parcel model (coded in Matlab). The model, which is described by Pruppacher and Klett (1997), solves the kinetic formulation for condensation of water on size resolved aerosol particles, based on the diffusional growth equation. The model is composed of essentially the same equations as the model developed in Leaitch et al. (1986) and later applied by Lohman and Leck (2005), with a few differences. Firstly, due to development of both computer hardware and software it is now possible to solve the full implicit ordinary differential equation system instead of earlier necessary simplifications. Secondly, measured size distributions of both number and chemical compositions are used as direct model input variables. The main advantage of this approach is that the observed mass and number aerosol size distributions are preserved. In the Leaitch et al. and Lohman and Leck studies the size distributions had to be transferred to a series of log-normal distributions with constant chemical composition, which caused a risk for loss of size resolved information. However, the uncertainty in mass that arises from the chemical analyses (Sect. 2.3) together with uncertainties connected with the measured growth factors (Sect. 2.4) still could influence our results. This is reflected in the error bars of Figs. 11 and 12. Finally, we identify that the Raoult term in the particle growth equation given in the Supplement is equal to $-\ln(a_w)$. Similar to Lohmann and Leck (2005), the model defines a CCN as a particle having a wet diameter $> 1 \mu\text{m}$ and a positive growth rate. The total simulation length was 50 s and set to correspond to the residence time of the particles in the CCN counter. For more detailed information on the modelling approach, please refer to the information in the Supplement.

4 Results of CCN measurements

4.1 Temporal changes of CCNC

Figure 2 gives a time series of the CCN observations (averaged over 1 minute) for water vapour SS of 0.2 % (sampler 1). Blue dots show CCNC measured at 0.17 % SS (DOY 216–228), while light blue dots show the CCNC at 0.21 % SS (DOY 229–253). Between days 216 and 218 the measurements were collected in the open sea or at the marginal ice edge of the Greenland Sea–Fram Strait area. The period between DOY 225 and 246 represents the ice drift period. Four features stand out: the CCNC were constantly below 100 cm^{-3} in the marginal over the pack ice, and occasionally below 1 cm^{-3} (described in Mauritzen et al., 2011); the 2–3 orders of magnitude overall range in concentrations from below $1\text{--}100 \text{ cm}^{-3}$; and changes in concentration, sometimes exceeding the entire seasonal variation, often occurred within an hour. This large temporal variability in the data is consistent with measurements from earlier high Arctic campaigns. Work by Bigg et al. (2001) has shown that the common stratification together with dynamic processes within the lower

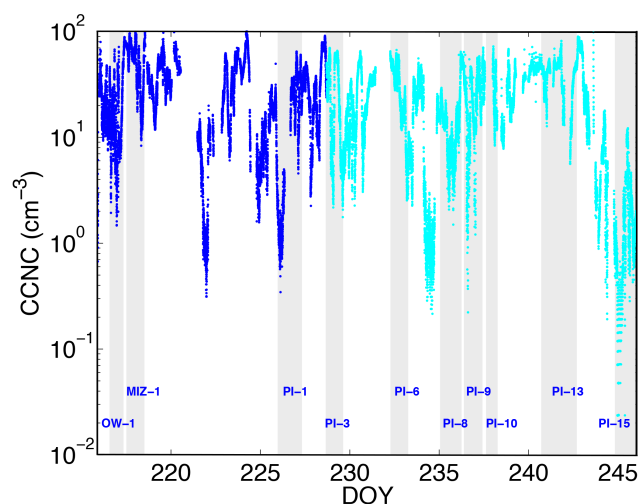


Figure 2. CCNC as a function of time in units of cm^{-3} . Blue dots show CCNC measured at 0.17 % water vapour SS; light blue dots show the CCNC at 0.21 % water vapour SS. The grey bars mark the duration of each of the impactor samples. Details on impactor start and stop times are given in Table 2.

part of the boundary layer exerts large influences on near-surface concentrations of aerosols in the central Arctic.

Median daily concentrations were ranging typically between 15 and 30 cm^{-3} but were a factor of 3 higher at the ice edge at latitude 80°N (days 216–218). At the location of the PI-drift station on days 244–245 the median concentration was a factor of 100 lower than on days 216–218, so a temporal change throughout the month of August of this magnitude may be buried in the noisy data. However, transport time from open water over the pack ice (referred to as DOI) is shown below to be important and may emphasize the temporal change.

4.2 CCNC changes with DOI and air mass origin

It has become clear from the above discussion that in order to understand the occurrence of CCNC in the atmosphere over the pack ice, an understanding of the synoptic scale systems advecting heat, moisture and particles from the surrounding open seas over the pack ice will be required.

Based on the availability of data from key instruments utilized in this study the following group of the impactor samples were included for further analyses: OW-1, MIZ-1, PI-1, PI-3, PI-6, PI-8, PI-9, PI-10, PI-13 and PI-15. The grey bars in Fig. 2 mark the duration of their respective sampling period. Table 2 gives more information on start–stop times and sample duration. The observed CCNC were averaged over the impactor sampling times and Table 2 tabulates the 25th, 50th (median) and 75th percentile CCNC separately for open water (OW-1), marginal ice zone (MIZ-1) and pack ice (PI-1, 3, 6, 8, 9, 10, 13 and 15) measurements at ca. 0.2 % SS (counter 1). During sample PI-1 and PI-10 we encountered

Table 2. The 25th, 50th (median) and 75th percentile CCNC separately for open water (OW-1), marginal ice zone (MIZ-1) and pack ice (PI-1, 3, 6, 8, 9, 10, 13, and 15) measurements at 0.2 % SS (counter 1). Values are at STP. Also listed are information on sampling start–stop times and sample duration and on the air trajectory cluster and average DOI during the sampling time for each of the impactors.

Sample	Start time DOY	End time DOY	Sampling location	Trajectory- cluster	DOI	CCNC 50th percentile cm^{-3}	CCNC 25th percentile cm^{-3}	CCNC 75th percentile cm^{-3}	Missing aerosol fraction
OW-1	216.561	217.342	Open water	–	NA	12.9	8.2	24.6	0.51
MIZ-1	217.503	218.508	Marginal ice zone	–	0	57.3	33.5	70.2	0.67
PI-1	225.967	227.321	Ice drift	1	2.5	17.4	1.8	31.7	0.46
PI-3	228.656	229.626	Ice drift	2	1.6	23.8	6.4	52.7	0.68
PI-6	232.272	233.269	Ice drift	1	4.6	29.4	15.5	45.7	0.68
PI-8	235.049	236.253	Ice drift	3	NA	13.0	6.9	16.8	0.40
PI-9	236.382	237.419	Ice drift	2	1.2	30.1	25.8	32.8	0.56
PI-10	237.625	238.271	Ice drift	2	1.4	23.8	15.5	41.4	0.31
PI-13	240.708	242.700	Ice drift	4	6.1	44.3	30.9	47.9	0.76
PI-15	216.561	217.342	Ice drift	5	9.3	0.95	0.40	2.1	0.57

episodes of pollution (cf. Fig. 2) during which all pumps automatically were closed. During the episodes the temporal records of the TDMPS observations seemed unchanged relative to before its start. We therefore will assume no systematic biases in the calculated median CCNC and that the chemical composition of the impactors is sufficiently compatible.

The backward trajectories shown in Fig. 3 were subjectively classified in four clusters depending on their geographical origin only. They were calculated for a receptor point of 100 m at the location of the ship. This allowed for an identification of impactor samples representing similar source regions. The origin of the air during both the 1st (PI-1 and PI-6) and 2nd (PI-3, PI-9 and PI-10) clusters was highly variable on a daily basis, as in the very synoptically active period during the first half of the expedition (Tjernström et al., 2012). The air trajectories of cluster 1 (Fig. 3a) originated easterly from the Barents and Kara seas. For cluster 2 (Fig. 3b) they came from the Fram Strait–Greenland Sea area. In both clusters the air spent a relatively short time over the ice (DOI \sim 2) since last contact with open sea. The period of trajectory cluster 1 (PI-1 and PI-6) and part of cluster 2 (PI-3) had numerous melt ponds on the ice surface, with temperatures around 0 °C. The ice-melt was followed by a drop in temperature to -6 °C for about 2.5 days and included the third trajectory cluster (PI-8). The air origin during the third cluster was mainly from Greenland (Fig. 3c). The vertical component of the air trajectories (not presented) shows a subsiding pathway from the free troposphere across Greenland to the surface, which suggests that the air sampled on board *Oden* was of free tropospheric origin. No DOI could be calculated since the trajectories did not have any contact with the open sea. After this brief snapshot of cold air, near-surface temperatures became semi-stationary around -2 °C and hosted part of the second trajectory cluster (PI-9 and PI-10). During the fourth (PI-13) and fifth (PI-15) clusters (Fig. 3d and e),

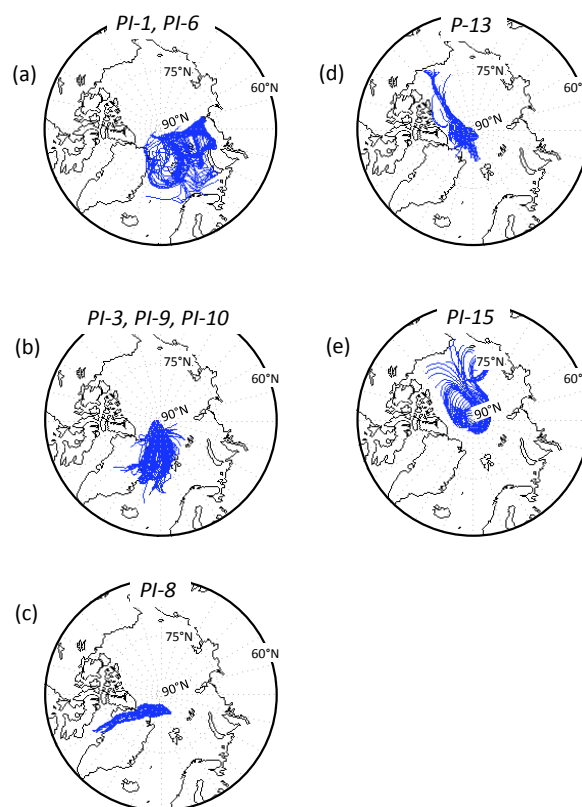


Figure 3. Air trajectory clusters with an arrival height of 100 m at the position of the icebreaker during: (a) cluster 1 (DOY 227, DOY 229–232) originated easterly from the Barents and Kara seas, (b) cluster 2 (DOY 228, DOY 236, 238–239) from the Greenland Sea–Fram Strait area, (c) cluster 3 (DOY 234–235) from Greenland, (d) cluster 4 from north-western circumpolar over the pack ice during DOY 240–243, and (e) cluster 5 from north-western circumpolar over the pack ice during DOY 243–246. Table 2 gives the calculated DOI for each of the impactors.

the air flow was largely from north western circumpolar over the pack ice for approximately DOI = 8 and from the direction of the Laptev and East Siberian seas towards the end of the period but still with no close contact with open sea. The conditions during the fourth trajectory cluster were governed by a persistent stratocumulus layer that contributed to maintaining the temperatures between -2 and -3 °C. The fifth trajectory cluster started on 31 August (DOY 244) and ended on 2 September (DOY 246) as the persistent stratocumulus layer went away and the clouds, if present, became optically thin (Mauritsen et al., 2010), which resulted a drastic drop in temperature to -12 °C and sunny conditions. During OW-1 (DOY 216–217) we experienced air predominantly from the ice-covered archipelago north of Canada and Alaska, without any contact with the open sea within 10 days. Therefore also in this case no DOI could be calculated. During MIZ-1 (DOY 217–218) the air crossed over open water along the east coast of Greenland prior to sampling at the location of the ship. Trajectories for OW-1 or MIZ-1 are not presented.

Figure 4 translates the time series of Fig. 2 and Table 2 into CCNC as a function of the synoptic scale systems since their last contact with open sea, defined as DOI. Perhaps the most important result contained in Fig. 4 is the loss of CCN approaching a factor of 3 during about the first 2 days of transport from the ice edge, followed by a recovery. Herman and Goody (1976) have modelled the formation of fog and cloud in warm moist air during advection over the pack ice. They concluded that advection fog formed on the first and second day over the pack ice but lifted to form low stratus on day 3. Losses of CCN to the surface in the surface mixed layer will therefore be expected to be at a maximum on the first and second days when drizzle and fallout of fog drops aid deposition to the surface, consistent with the steep decline seen in Fig. 4 and with previous reported studies in the same area and season (Bigg and Leck, 2001a). Thereafter losses should have continued by wet deposition at a lower rate, but we actually see an increase in number of CCN in two of the three impactor samples (PI-6 and PI-13, Table 2) for DOI > 4. This feature is again consistent with previous work by Bigg and Leck (2001a) and indicative of a source of CCN particles in the inner Arctic.

One other much less frequently occurring (a few days out of a 40 days expedition in total) possible cause of the CCNC increase, represented by sample PI-13 (DOI=6.1, Table 2), is coinciding with a recoupling and turbulent mixing between a shallow (~ 150 m deep) surface-based mixed layer and a separate mixed layer located in the upper part of the boundary layer, which contained stratocumulus clouds (more details in Shupe et al., 2013). The backward trajectory analysis suggests that the air in the upper boundary layer had come from the Canadian archipelago (not shown) while that in the lowest 100 m (shown in Fig. 3d) had been over the ice for at least 10 days. Based on the CCN fingerprint we therefore speculate that the surface air that mixed with the upper part of the boundary layer was influenced by continental sources.

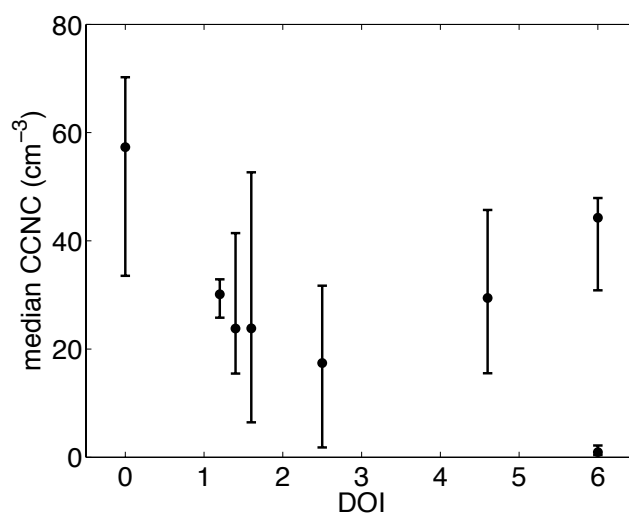


Figure 4. Median (50th percentile) CCNC for the duration of the impactor samples as a function of travel time over ice (DOI, days). Data for all travel times of 5 days and longer have been collected at 6 days. Error bars indicate 25th and 75th percentiles.

Several studies from ASCOS support this finding (Paatero et al., 2009; Chang et al., 2011; Leck et al., 2013; Kupiszewski et al., 2013; Sierau et al., 2014).

The extremely low CCNC (median levels of 1 cm^{-3} , about 200 nm in diameter for a water vapour SS at 0.2 %) observed during PI-15 (DOI = 9.3, Table 2) is related to the meteorological conditions (Fig. 3e) and aerosol stratification prevailing during the time of sampling of PI-15. Based on the helicopter profiles observed during ASCOS, Kupiszewski et al. (2013) report on concentrations of aerosol particles of ca. 300 nm in diameter, being very low (0.5 cm^{-3}) within the lowermost few hundred metres. Starting on the second half of 31 August the TDMPS measurements on board *Oden* also showed a strong decrease in accumulation mode particle concentration to below 1 cm^{-3} . The low aerosol particle concentrations were accompanied by an almost complete disappearance of clouds, which was observed from ca. 20:00 UTC on 31 August. Mauritsen et al. (2011) hypothesize that the cause of the tenuous cloud regime is that when the CCNC fall below some critical value, droplets grow large and rapidly sediment out. This contributes both to keeping the CCNC low, by the removal of the CCN, and to removing cloud water, thus keeping the clouds optically thin. An analysis of corresponding CCN data from the previous three *Oden*-based expeditions (Mauritsen et al., 2011) showed that this kind of tenuous cloud regime occurred about 25 % of the time.

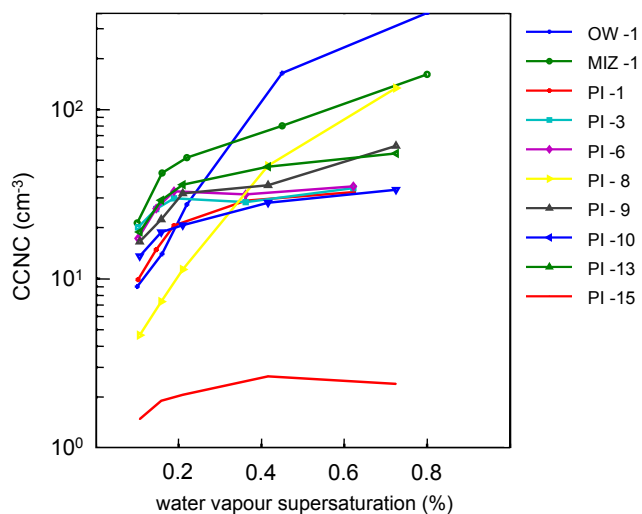


Figure 5. The measured CCNC as a function of the choice of water vapour SS (five levels between 0.1 and 0.8 %) as seen by the second CCN sampler. The data are shown separately for open water (OW 1), marginal ice zone (MIZ 1) and pack ice (PI-1, 3, 6, 8, 9, 10, 13, and 15) measurements.

5 The sensitivity of CCNC as a function of water vapour SSs

5.1 Measured CCNC as a function of water vapour SSs

Figure 5 displays the sensitivity of measured CCNC (averaged over the duration of each of the impactor samples) as a function of the five levels of water vapour SS between 0.1 and 0.8 % seen by the second CCN counter. Increasing the water vapour SS from 0.1 to 0.2 % resulted in a significant increase in CCNC for all impactor samples, but further SS increases resulted in small or non-existent change in CCNC for samples PI-1, PI-3, PI-6, PI-9, PI-10 and PI-13, respectively. This feature was also seen in Sample PI-15 but at a much lower absolute level.

Figure 6 displays the variation in CCNC with increasing water vapour SS normalized to the average values for the duration of each of the impactor samples. The similarity in the shape of CCNC as a function of SS is seen for the PI-1, PI-3, PI-6, PI-9, PI-10, PI-13 and PI-15 impactor samples (Fig. 6 lower panel). It should be noted that the temporal variability in CCNC covered by each of the impactors is high (Fig. 2 and Table 2) and since the measurements for each SS only cover about 20 % of the time within the start and stop times of the impactors, systematic biases could result. However, since all the seven samples are showing similar features there is no evident reason to suspect systematic biases. The OW-1 and PI-8 samples, pictured in Fig. 6 (upper panel), show on the other hand a more or less continuous increase in CCNC with increasing water vapour SS. A similar but weaker continuous increase in CCNC with increasing water SS was also shown for sample MIZ-1 plotted in Fig. 6 (upper panel).

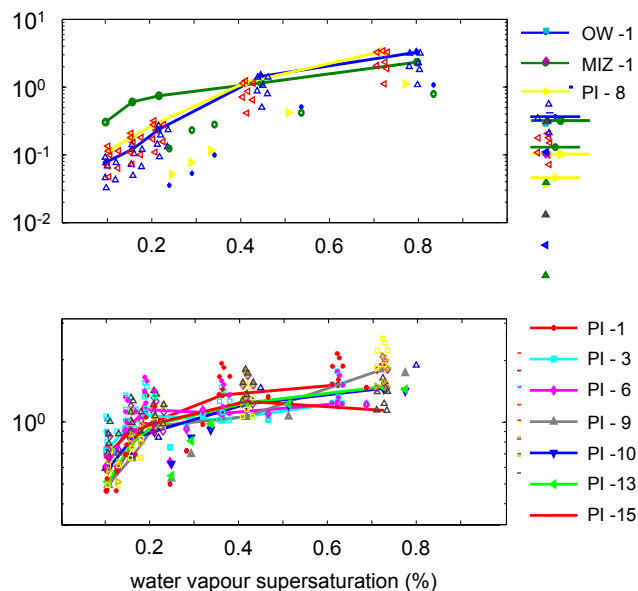


Figure 6. Variation in CCNC as a function of water vapour SS (as in Fig. 5) normalized to the average CCNC value for the duration of the impactor samples.

In view of the observed sensitivity of measured CCNC as a function of water vapour SS the characteristics of the impactor samples could be summarized as follows: (1) OW-1 and MIZ-1 with more or less continuous increase in CCNC with increasing water vapour SS. The air origin was predominantly from the ice covered archipelago north of Canada and Alaska and from over open water along the east coast of Greenland, (2) pack ice sample PI-8 with a similar feature as of (1). Sample PI-8 collected air with possible free tropospheric origin (cluster 3: Fig. 3c), (3) samples PI-1, PI-3, PI-6, PI-9, PI-10, PI-13 and PI-15 which all showed a small or non-existent continuous change in CCNC with increasing water vapour SS > 0.2 %. One common feature for five out of the seven impactor samples was that the sampled air spent a relatively short time over the ice (DOI \sim 2) since last contact with open sea. The origin of the air during PI-1 and PI-6 (trajectory cluster 1: Fig. 3a) and PI-3, PI-9 and PI-10 (cluster 2: Fig. 3b) were easterly from the Barents and Kara seas and from the Fram Strait–Greenland Sea area. For the remaining two samples PI-13 (cluster 4: Fig. 3d) and PI-15 (cluster 5: Fig. 3e), the air was advected over the pack ice for more than 6 days since contact with open sea.

At first sight the above results suggested that either differences in time of advection of the air over the pack ice or possible impact from non marine aerosol sources, as in PI-8, did have any systematic affect on the sensitivity of observed CCNC as a function of water vapour SS.

To further search for a relationship between the properties of the summer high Arctic aerosol and its ability to form CCN, we will use observed aerosol number size distribution data, additional hygroscopic growth information, and deter-

mined aerosol bulk chemistry resolved over size. We will focus mainly on five samples as representatives for the features summarized above: MIZ-1, PI-1 (trajectory cluster 1), PI-8 (trajectory cluster 3), PI-10 (trajectory cluster 2) and PI-15 (trajectory cluster 5).

5.2 κ -Köhler theory predictions

We next derived aerosol activation-limit dry diameter from the measured CCN number concentrations and TDMPS size distributions by only assuming that larger particles will activate at lower water vapour SS than smaller particles. The derived diameters were compared to κ -Köhler theory (Petters and Kreidenweis, 2007) using a range of κ values and $\sigma_{s/a}$, assuming a size-independent aerosol chemical composition. Assumed κ values ranged from 0.1 to 1. Based on the determined chemical composition of the impactor samples, κ values below 0.1 were not included in the comparison. The aerosol surface tension was also assumed to be size-independent and equal either to that of pure water ($\sigma_{s/a} = 73 \text{ mN m}^{-1}$ at 20°C) or to a value of $\sigma_{s/a} = 50 \text{ mN m}^{-1}$ representing a case of moderate particle surface activity.

Figure 7 shows that the aerosol activation-limit dry diameter of the samples generally tended to be larger than the expected diameters from the assumed pairs of κ - and $\sigma_{s/a}$. At lower water vapour SSc and in general for impactor samples MIZ-1, PI-1 and PI-8, the mismatch was less severe. The predictions showed clearly that impactor PI-10 and PI-15 deviate the most from the κ -Köhler theory, with a shown increase of the hydrophobic character in the activated particles with decreasing diameter, with impeded water uptake as a consequence.

To further study which aerosol properties possibly could suppress cloud droplet formation with decreasing diameter, we will continue to simulate cloud nucleation assuming Köhler theory. The Köhler theory will be combined with a Lagrangian adiabatic air parcel model that solves the kinetic formulation for condensation of water on size resolved aerosol particles. For details on the approach, please refer to the Supplement. In Sect. 8 the CCNC simulations will use the observed aerosol number size distribution data and assumptions on the composition on the inorganic/organic aerosol system resolved over size. In the later case the water soluble determined impactor data will be used together with a best guess of the properties of the “missing non-water soluble fraction”, that is the fraction of particles not classified by the chemical determinations. Before presenting the results from the CCNC simulations in Sect. 8, Sects. 6 and 7 will discuss how to assume the “missing non-water soluble” aerosol fraction using a comparison between the TDMPS number size distribution and the converted total water soluble mass determined by the impactors.

6 Size resolved aerosol water soluble chemical composition by number

Figure 8 displays a comparison between the converted total water-soluble mass determined by the impactors and the TDMPS number size distribution. Figure 9 gives additional details on the ionic contribution of Ca^{2+} , Na^+ , Cl^- , SO_4^{2-} and MSA to the total water-soluble mass determined.

Impactor sample PI-10: the average number size distribution collected during impactor sample PI-10 showed a strong bimodal distribution (Fig. 8, PI-10), with the Aitken and accumulation modes possibly separated by a Hoppel minimum (Hoppel et al., 1994). This is a known characteristic of an aerosol population modified by cloud/fog processing (Hoppel et al., 1986) and originating over a marine area (Heintzenberg et al., 2004). The fact that the air trajectory cluster (Fig. 3b) originated predominantly from the MIZ of the Fram Strait–Greenland Sea area in foggy conditions provides a coherent picture.

Guided by findings from past *Oden* expeditions (Karl et al., 2012; Kerminen and Leck, 2001; Leck and Bigg, 2005b; Leck and Persson, 1996; Leck et al., 2002), we suggest that the pronounced accumulation mode in part resulted from condensational growth on pre-existing Aitken mode particles from precursor gases such as the DMS oxidation products with subsequent activation as cloud droplets. Activated particles could then have grown via in-cloud aqueous phase oxidation of gases such as sulfur dioxide (SO_2), resulting in release of larger particles following droplet evaporation (Lelieveld and Heintzenberg, 1992). Figure 9 (PI-10) confirms the expected large fraction of the oxidation products of DMS (SO_4^{2-} and MSA) to total analysed water soluble constituents in the accumulation mode. When the air has been in very recent contact with the MIZ/open water ($\text{DOI} = 1.4$, Table 2), a further mechanism would have involved the release of accumulation mode primary marine particles (sea salt and biogenic) from the MIZ via bubble bursting (Nilsson et al., 2001; Leck et al., 2002; Bigg and Leck, 2008). The sea salt contribution to the accumulation mode of the PI-10 water soluble aerosol fraction is shown in Fig. 9 (PI-10).

Impactor samples MIZ-1 and PI-1: a similar strong bimodal distribution with the Aitken and accumulation modes separated with a Hoppel minimum was seen in samples MIZ-1 and PI-1 (Fig. 8, MIZ-1; PI-1). Their accumulation modes were however less developed relative to the Aitken mode compared to sample PI-10, which would suggest an aerosol to a lesser extent modified by in-cloud processing via in-cloud aqueous phase oxidation of SO_2 . Figure 9 (MIZ-1) shows that sea salt from bursting bubbles at the sea–air interface also contributed to the water soluble fraction in the Aitken and accumulation modes. In a parallel study during ASCOS by Leck et al. (2013; Fig. 4 in that paper, middle panel) the additional contribution of particulate polysac-

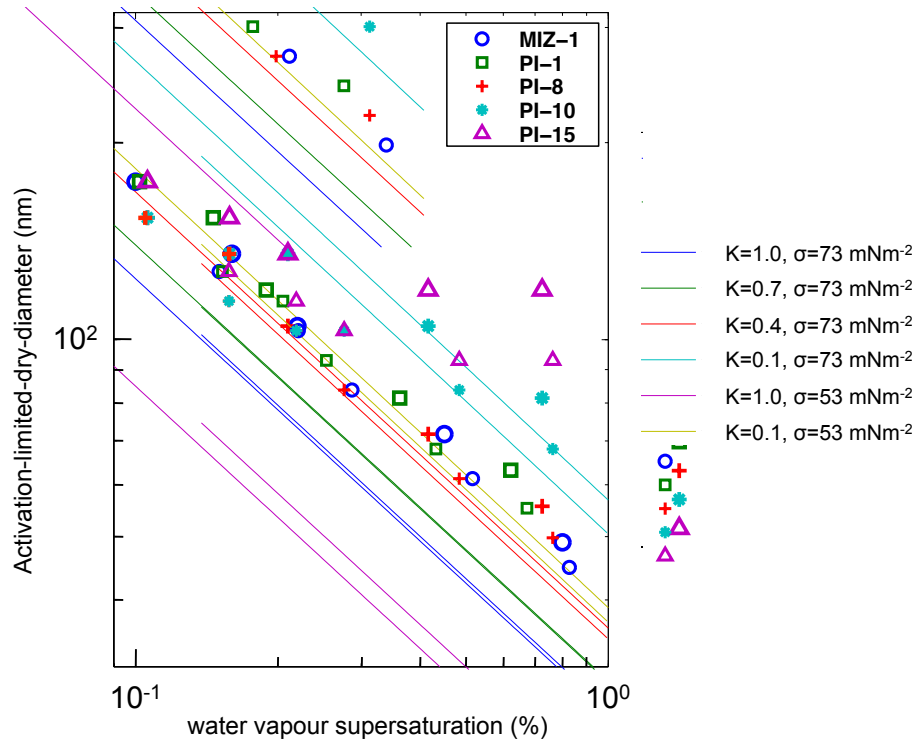


Figure 7. κ -Köhler theory predictions of the aerosol activation-limit dry diameter for assumed pairs of κ and σ (lines) compared to values derived from the impactor samples MIZ-1, PI-1, PI-8, PI-10 and PI-15 (symbols).

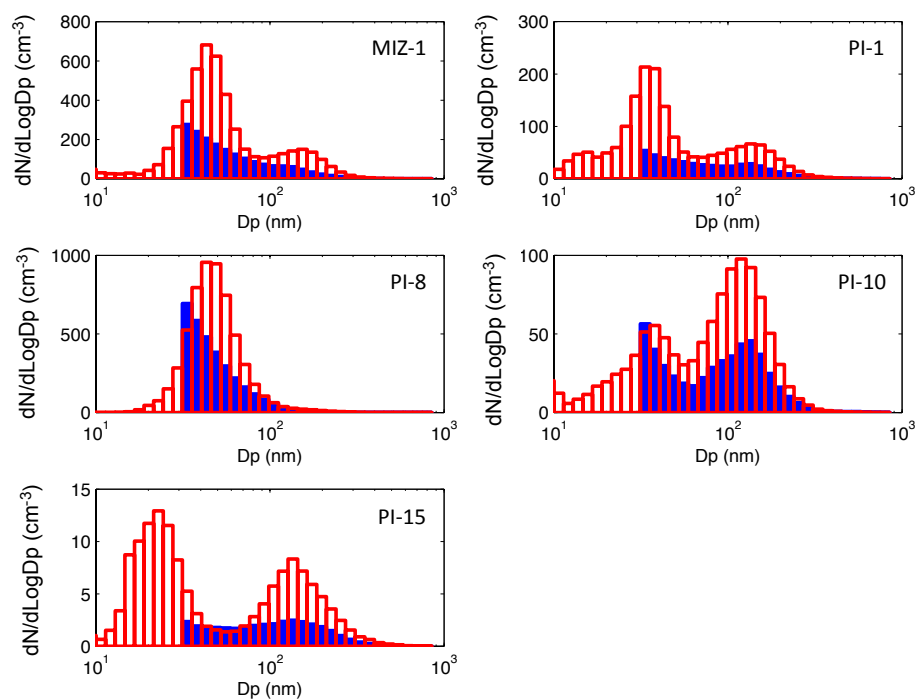


Figure 8. Comparison between TDMPS number size distribution (red) and converted mass size distributions (blue) for samples MIZ-1, PI-1, PI-8, PI-10 and PI-15.

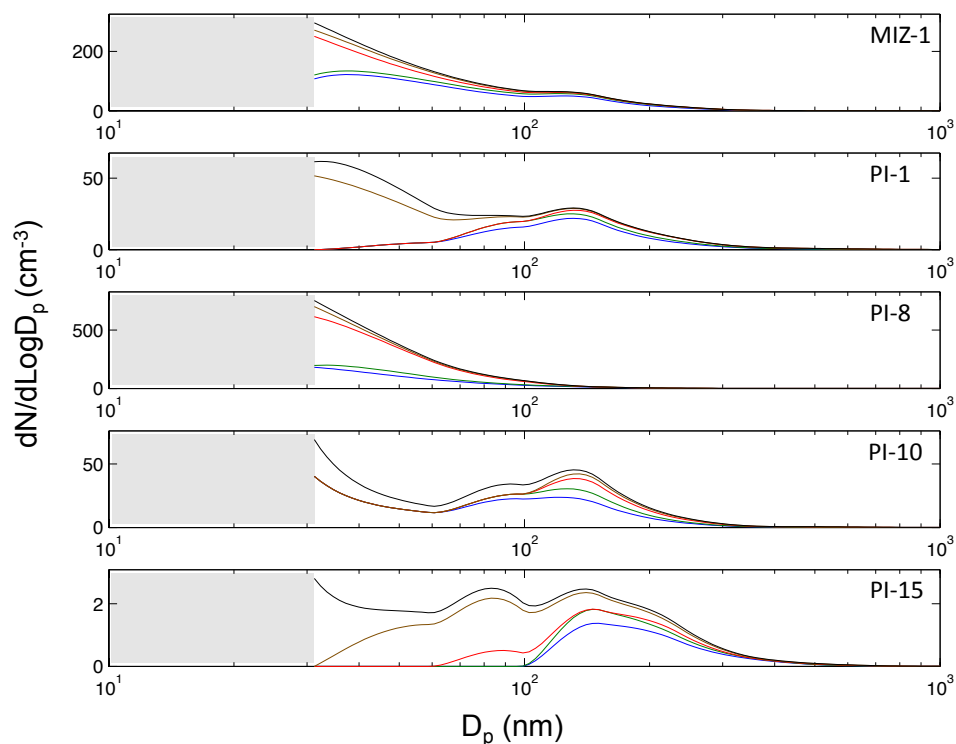


Figure 9. Number concentrations derived from impactor mass data. Blue lines show sulfate only, green lines sulfate + MSA, red lines sulfate + MSA + Na^+ + Cl^- , brown lines sulfate + MSA + Na^+ + Cl^- + Ca^{2+} , and black lines show the total analysed concentration.

charides (building blocks of polymer gels⁴) from the same bubble bursting mechanism can be seen⁵. The dominance of Ca^{2+} for sub-accumulation mode particle seen in Fig. 9 (PI-1) indirectly suggests the presence of polysaccharide molecules inter-bridged with divalent ions. A domination of Ca^{2+} for smaller particles was also observed in samples PI-10 and PI-15.

Impactor sample PI-15: the impactor sample PI-15 shared the bimodal characteristics of samples PI-10, PI-1 and MIZ-1, but at a much lower absolute number concentration and with a wider minimum between the accumulation mode and a sub-Aitken mode; see Fig. 8 (PI-15). The extremely low CCNC observed during PI-15 was discussed in Sect. 3.2 as being related to the prevailing meteorological conditions (Fig. 3e) and aerosol stratification (Kupiszewski et al., 2013). Below 10 nm (not shown in Fig. 8, PI-15) a strong mode of recent nucleated particles was observed. In addition, the

⁴Marine gels or polymer gels are produced by phytoplankton and biological secretions of sea ice algae at the sea–air interface. The polymer gels are made up of water insoluble, heat resistant, highly surface-active and highly hydrated (99% water) polysaccharide molecules spontaneously forming 3-dimensional networks inter-bridged with divalent ions (Ca^{2+} / Mg^{2+}), to which other organic compounds, such as proteins and lipids, are readily bound (Verdugo, 2012 gives a review).

⁵The limited mass collected by the highly size resolved LPI impactors did not allow for analysis of polysaccharides.

measurements showed that the availability of condensable vapours was limited in the boundary layer during PI-15, and that the concentration of DMS (below 4 ppt (v)), a precursor to sulfuric acid, was not sufficient to sustain growth into the super 10 nm diameter size range. This also left unexplained the observed co-appearance of particles in the 20–50 nm diameter size range coinciding with the nucleation. To explain the nucleation event Karl et al. (2013) suggested a novel route to atmospheric particle generation that appears to be operative during PI-15. It involves the fragmentation of primary marine polymer gels into the air from evaporating fog and cloud droplets. The ionic composition of the sub-accumulation mode of sample PI-15 was shown to be negligible in not only the sulfur containing but also all other water soluble constituents except Ca^{2+} (Fig. 9, PI-15). This observation supports the findings by Orellana et al. (2011) and Leck et al. (2013), who observed polymer gels in atmospheric samples during the course of PI-15. Sulfur components and Ca^{2+} dominated the accumulation mode. In view of the above discussion polymer gels could potentially have contributed to the missing non-water soluble fraction not only in PI-15 but also in samples MIZ-1, PI-1 and PI-10.

Impactor sample PI-8: the single Aitken mode distribution of PI-8, peaking at 45 nm diameter (Fig. 8, PI-8), suggests an aerosol population sourced in the free troposphere (Leck and Persson, 1996). The air trajectory in Fig. 3c showing a subsiding pathway from the free troposphere across Greenland

to the surface also points to air of free tropospheric origin. The low marine biogenic factor calculated for ASCOS by Chang et al. (2011) again consistently suggests air arriving at the surface without recent contact with the marine influenced boundary layer. Note the high contribution of Na^+ and Cl^- and Ca^{2+} . This likely free tropospheric origin of PI-8 limits our knowledge of possible aerosol sources and thus of candidates for the missing non-water soluble fraction seen in Fig. 8 (PI-8).

7 Assuming the missing non-water soluble aerosol fraction

Guided by the size resolved bulk chemical information given in Fig. 9 and bulk chemical and electron microscope analyses not only from ASCOS (Chang et al., 2011; Hamacher-Barth et al., 2013; Karl et al., 2013; Leck et al., 2013; Orellana et al., 2011) but from all three previous expeditions in the summers of 1991, 1996 and 2001 (Bigg and Leck, 2001a, 2001b, 2008; Leck and Persson, 1996; Leck and Bigg, 1999, 2005a, b, 2010; Leck et al., 2002; Lohman and Leck, 2005), we will assume the sub-Aitken mode particles (Fig. 10a–c) to be made up of externally mixed organically derived small polymer gels with hydrophobic and hydrophilic properties to various degrees (Xin et al., 2013; Orellana et al., 2011). Statistical analysis of the aerosol size distribution data collected over the inner Arctic recorded in the years 1991, 1996, 2001 and 2008 classified 17 % of the observed time period to be characterized by the spontaneous appearance of several distinct size bands below 50 nm diameter as discussed in Karl et al. (2013). However, there appears to be an inconsistency when comparing observations of small particle formation over the inner Arctic and those south of the pack ice area. The studies at Alert, Canada (82.5° N; 62.3° W) and Ny-Ålesund, Svalbard (79° N; 11.9° E) in spring and early summer by Engvall et al. (2008) and Leaitch et al. (2013) showed nucleation events followed by subsequent growth, which could be explained by solar radiation in concert with the presence of precursor gases and attendant low condensational sinks. Possible reasons for the inconsistency could be that the DMS source and photochemical sink generating the precursor gases for nucleation and early growth are both seasonal and temperature dependent (Leck and Persson, 1996; Kerminen and Leck, 2001; Karl et al., 2007; 2012). Given that, perhaps the main difference between the studies concerns how efficiently nucleation and growth of particles resulting from DMS oxidation are predicted by the choice of model and lack of observations to constrain the assumptions made.

As the sub-Aitken particles grow, we will assume the particles result from deposition of acids/organic vapours on a polymer gel-aggregate (Fig. 10d, e) or are typical of a sulfur-containing particle with hygroscopic properties in which any nucleus has become obscured by the surrounding of a

sulfate–methane sulfonate–ammonium complex (Fig. 10f). The Aitken mode and smaller accumulation mode below ca. 100 nm in diameter will be assumed to be represented by external mixtures of gels and internally mixed sulfur constituents (Fig. 10g), whereas accumulation mode particles at a few hundred nanometres diameter will be assumed to be internal mixtures of gels and sulfur constituents.

Finally, the upper end of the accumulation mode above 200 nm in diameter will be assumed to be composed of internal mixtures resulting from multiple sources, as in Fig. 10h, showing sea salt and a bacterium coated with an organic film and the concentric rings typical of droplets of sulfuric acid. In addition, film drops could add gel material with salt-free water with or without any attached microorganism; Fig. 10i shows an example of the latter. In Bigg and Leck (2008) it was suggested that the highly surface-active polymer gels could attach readily to the surface of rising bubbles and self-collide to form larger aggregates. Consequently, polymer gels and their aggregate production, as well as the embedded solid particles such as bacteria, phytoplankton and its detritus, can be carried selectively to the surface microlayer by rising bubbles. Before bursting, bubbles stay in the microlayer for some time and therefore are likely to acquire walls, consisting to a large extent of strengthening gels, with embedded particulate matter that may be points of weakness as the water drains from between the walls. Following the burst, the film drop fragments would not be drops of salt water but of gel material with salt-free water and any particles attached to the fragments. Previous reported results of individual particles by Bigg and Leck (2001b, 2008), Leck et al. (2002) and Leck and Bigg (2005a, 2005b, 2010) collected over the pack ice have failed to find evidence of sea salt particles of less than 200 nm diameter. The presence of bubbles observed in the water column (Norris et al., 2011) provides a plausible mechanism for getting surface material airborne. In all, this supports the suggested mechanism for getting the primary biogenic material at the open-lead⁶ surface airborne. Even though jet drop particles (“jet drops”: centred around 1 μm diameter) are mainly composed of sea salt, they have been observed over the Arctic pack ice area to be partly coated by polymer gels (Leck et al., 2002). An example is seen in Fig. 10h.

For each of the impactor samples the “missing non-water soluble fraction” not classified by the chemical determinations is listed in Table 2, being on average 54 %. The fractions were derived from the difference between the observed total particle concentration seen by the TDMPS and the estimated total number concentration based on the chemical determinations.

As a surrogate for the unexplained fraction assumed to be organic (gels and condensed organic vapours) we will

⁶The high Arctic open leads can be described as ever-changing open water channels comprising 10–30 % of the ice pack ice area, ranging from a few metres up to a few kilometres in width.

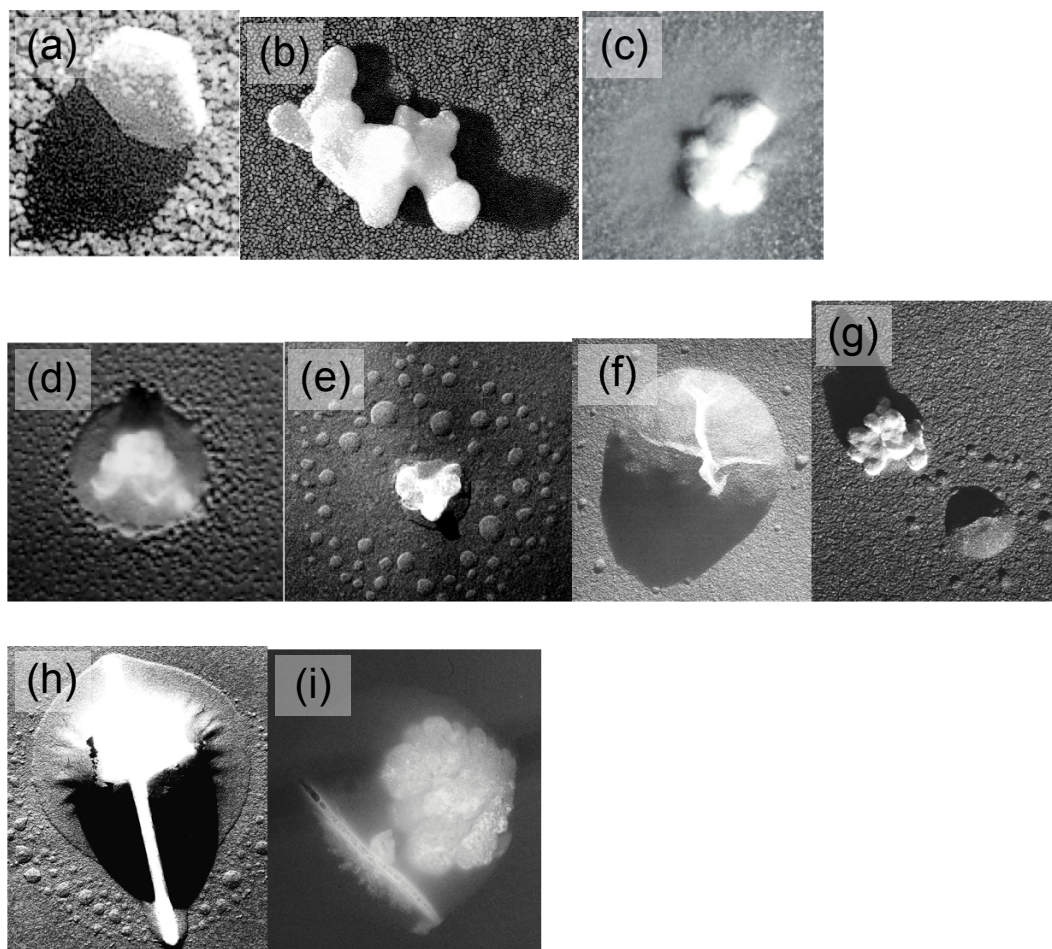


Figure 10. Examples of the changing nature of the high Arctic particles in different modal diameters: (a–c) sub-Aitken mode, (a) pentahexagonal structure, crystalline and hydrophobic in nature assumed to be a colloidal building block of a polymer gel, (b) small polymer gel-aggregate slightly covered with hydrophilic mucus, (c) same as in b but with more mucus remaining promoting its hydrophilic properties, (d–g) Aitken to small accumulation mode, (d) particle with a high sulfuric acid content with a gel-aggregate inclusion embedded in a film of high organic content, (e) gel-aggregate with satellites, indicating the presence of organics and acids, (f) particle containing mainly ammonium sulfate and methane sulfonate, (g) external mixture of a gel-aggregate and similar particle as of (f), and (h–i) large accumulation mode, (h) sea-salt particle with an organic content. The rod through its centre is assumed to be a bacterium. The particle has an acquired coating of sulfuric acid, (i) a gel-aggregate containing a bacterium attached to a small aggregate possibly detached from the larger one. The particles' bubble-like shape indicates a possible recent injection to the atmosphere at the air–sea interface.

use slightly water soluble and non-water soluble proxy constituents. As a slightly water soluble but moderately surface-active dicarboxylic acid we used adipic acid, which has been observed in ambient particulate matter including in the Arctic (Narukawa et al., 2002). Also detected in Arctic aerosol particles (Fu et al., 2009) was *cis*-pinonic acid, which was chosen as a surrogate for highly surface-active properties of the missing fraction with insignificant lowering of the water activity. Predicting a surface tension of mixtures of ionic solutions with surface-active organics is an ambiguous task. Inorganic components may either enhance or inhibit the surface tension depression caused by surfactants, depending on both concentration and substance (Tuckermann, 2007). Hence, a single best scheme to predict surface ten-

sion of mixed aqueous solutions is not likely to exist. In this study we set the aerosol surface tension for adipic acid to $\sigma_{s/a} = 68 \text{ mN m}^{-1}$ (Lohmann and Leck, 2005) and use a value of $\sigma_{s/a} = 38 \text{ mN m}^{-1}$ in the case of *cis*-pinonic (Tuckermann, 2007). The surface tension of the internally mixed accumulation mode aerosol was obtained by weighting the surface tension of each soluble constituent by its mass fraction.

Table 3 lists the various assumptions concerning the “missing non-water soluble fraction” used in the modelling, idealized for one size bin of a wet aerosol. The wet aerosol is in general assumed to consist of three more or less non-water soluble units with known determined water soluble constituents and 1/3 of dry mass not being determined. Dia-

Table 3. Assumptions on the missing non-water soluble aerosol fraction used in the simulations. The droplet bulks show increasing ionic concentration moving from grey to blue. Orange and red droplet fringes show various degrees of depressions in surface tension, red being the strongest. Grey diamonds represent a core of water insoluble particles.

Simulation	Illustration	Description
AD		Missing fraction behaves like internally mixed adipic acid; low water solubility and moderate surface active.
PIN		Missing fraction behaves like internally mixed <i>cis</i> -pinonic acid; low water solubility and highly surface active.
INSOL		Missing fraction behaves like a water insoluble particle inside the droplets; no surface activity.
SOL		Missing fraction is assumed to be non-existent, only the determined chemical size distribution is used.
AD_ext		The analysed part is externally mixed with an aerosol consisting of adipic acid.
PIN_ext		The analysed part is externally mixed with an aerosol consisting of <i>cis</i> -pinonic acid.

monds inside the droplets indicate a water insoluble particle fraction. The colour scale of the droplet bulks (from grey to blue) shows increasing ionic concentration, equivalent to a lowering of water activity. Orange and red droplet fringes show various degrees of depression in surface tension, red being the strongest.

For the INSOL simulation the missing fraction is assumed to be either a completely water insoluble core (Fig. 10d and h: gel or a bacterium) within the water soluble droplet or a sulfur-containing particle in which any gel-nucleus has become obscured by the surrounding of a sulfate–methane sulfonate–ammonium complex (Fig. 10f) was captured.

In the AD (low water solubility and moderate surface activity) and PIN (low water solubility and high surface activity) cases, particles are resulting from deposition of organic vapours on a polymer gel particles. Figure 10e shows an example.

When the externally non-water soluble fraction is assumed to be made up by pure adipic and/or *cis*-pinonic acid (AD_ext and PIN_ext respectively) it mimics the behaviour of a polymer gel (Fig. 10b and c; upper left of Fig. 10g–j), with interaction shown of its hydrophilic and hydrophobic entities (Orellana et al., 2001; Xin et al., 2013). The proportion between AD_ext and PIN_ext was linearly combined, assuming for example a 50 / 50 adipic / *cis*-pinonic acid external particle mixture.

The SOL assumption takes only the chemically determined water soluble aerosol fraction into account. This then represents an externally mixed aerosol with the water-

soluble, detected compounds as one part (2/3) and a completely CCN-inactive part (1/3) as the other (Fig. 10a).

8 Predicting CCNC

In the following section, we will present and discuss the results from the simulations in the order of PI-1, PI-8, PI-10, PI-15 and MIZ-1. Figure 11 is a compilation of all simulations. First to be noted is that the modelling results in the PIN case, where the missing fraction was assumed to behave like an internally mixed *cis*-pinonic acid, with low water solubility and highly surface active, consistently over-predicted the observed CCNC for all five impactor samples. These runs are therefore excluded in Fig. 11.

Impactor sample PI-1: according to the aerosol activation-limit dry diameters shown in Fig. 7, the scans at the three lowest water vapour SSs (0.10, 0.15, 0.20 %) activated particles within the accumulation mode. For the two highest levels of water vapour SS (0.37 and 0.62 %), particles within the Hoppel minimum down to ca. 60 nm in diameter were activated (Fig. 8, PI-1). As shown in Fig. 11 (PI-1) the simulation runs including the SOL, AD_ext and PIN_ext assumptions of the non-water soluble missing fraction were all able to capture the observed CCNC within 1 standard deviation ranging from 0.10 to 0.62 % water vapour SS. The shown activation for particles with decreasing diameter argues for a relatively increased influence of external mixtures of Fig. 10a–c type particles at the large-end tail of the Aitken mode. Also the case AD and INSOL did in general capture the observed

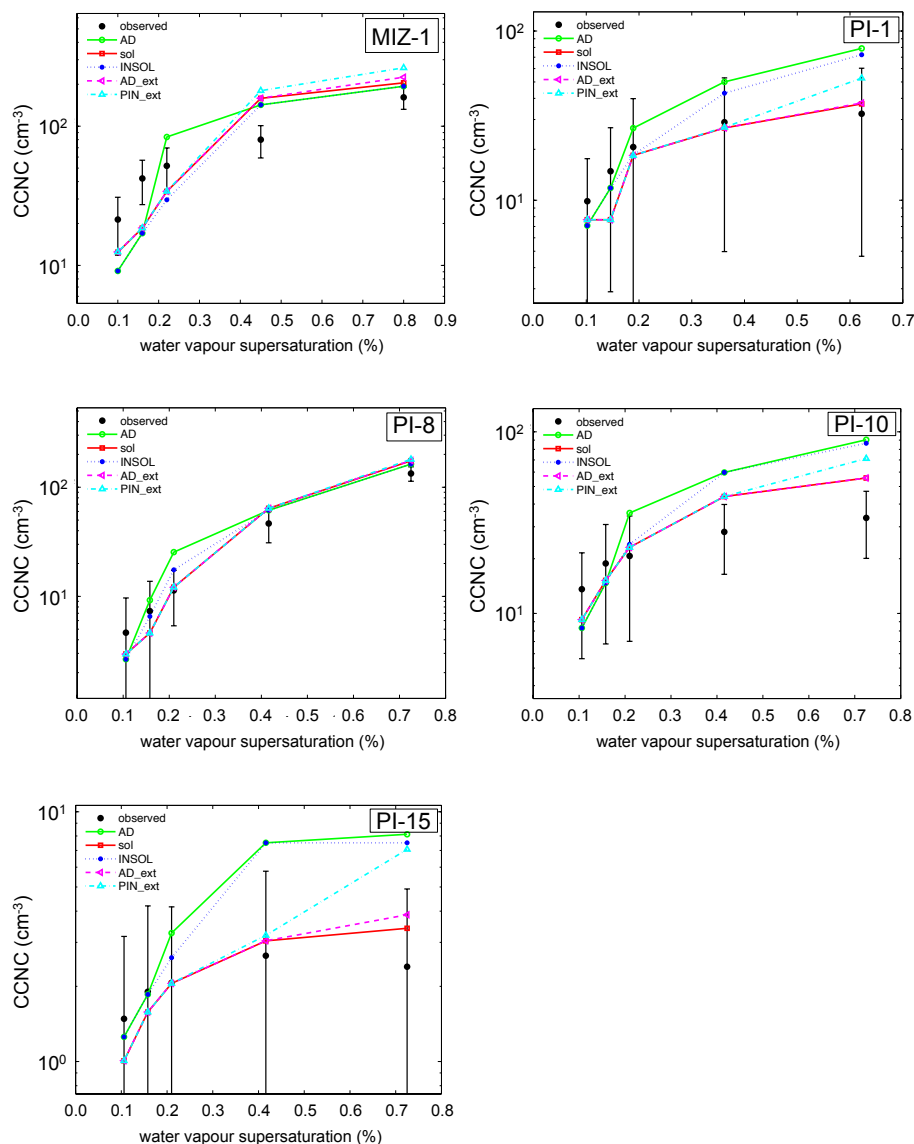


Figure 11. Observed and simulated CCNC for sample MIZ-1, PI-1, PI-8, PI-10 and PI-15, ranging from 0.1 % to 0.8 % water vapour SS. Error bars represent 1 standard deviation.

CCNC but over-predicted the CCNC for the highest level of SS. Hence, the aerosol in the accumulation size range was suggested to be mixtures of the type of particles exemplified in Fig. 10g–i but possibly also of type 10d–f.

Impactor sample PI-10: based on the aerosol activation-limit dry diameters for PI-10 (Fig. 7) the scanning, with all five water vapour SSs (0.10, 0.15, 0.20, 0.41 and 0.73 %) included, activated the accumulation mode particles down to ca. 80 nm diameter.

Similarly to PI-1, all assumptions of the non-water soluble missing fraction were able to reproduce the observed CCNC within 1 standard deviation below 0.20 % water vapour SS (Fig. 11, PI-10). However, all calculations above 0.20 % SS over-predicted the observed CCNC. This result indicates that

neither using the most conservative assumption on the missing fraction (INSOL: internal mixture with a completely insoluble and non-surface active core) nor using the assumption of an externally mixed aerosol with 2/3 being water soluble and 1/3 being completely CCN-inactive could predict the sensitivity of the observed CCNC as a function of water vapour SS.

Impactor sample PI-15: for particle sizes above 10 nm in diameter, PI-15 shared the bimodal characteristics with samples PI-1 and PI-10, but with a wider minimum between the accumulation mode and a sub-Aitken mode (Fig. 8, PI-15). As the extremely low (usually below 0.5 cm^{-3}), aerosol particle concentrations resulted in an almost complete disappearance of low clouds (Mauritsen et al., 2011) and clear

skies during the duration of PI-15, the minimum is primarily not a result of an aerosol population modified by in-cloud/fog processing (Hoppel et al., 1986). Instead the results by Gao et al. (2012), Leck et al. (2013) and Orellana et al. (2011) suggest that the accumulation mode instead was maintained by gel particles sourced from the open-lead surface microlayer.

Based on the aerosol activation-limit dry diameters for PI-15 (Fig. 7), the CCN-counter activated particles within the accumulation mode between 130 to 200 nm in diameter. The simulations in Fig. 11 (PI-15) showed that the SOL and AD_ext assumptions gave the best overall fit to the observed CCNC. It can be argued that the activated fractions of the accumulation mode encompassed an external mixture of particles with internal mixtures of water soluble constituents strong in DMS-derived sulfur and particles entirely CCN-inactive. An alternative explanation could be that the water uptake was impeded and perhaps requires longer than 50 s wetting/growth time in the CCN-counter. The latter property is consistent with the increase of the hydrophobic character in the activated particles with decreasing diameter seen in Fig. 7 (PI-15). In agreement with the observed and modelled chemical behaviour of the high Arctic polymer gels with their hydrophilic and hydrophobic segments (Orellana et al., 2011; Xin et al., 2013), water vapour does not uniformly condense on the gel since only part of the surface exhibits strong hydrophilicity. Thus, as discussed above, the polymer gels would be expected to show initially only partial wetting character below 100 % RH but given enough time a high CCN activation efficiency, which is promoted by its surface-active properties (cf. the PIN_ext case in Fig. 11, PI-15) of the gels (Ovadnevaite et al., 2011).

Impactor sample PI-8: as identified above, sample PI-8 was the only sample of all those collected in the pack ice with a more or less continuous increase in CCNC with increasing water vapour SS. PI-8 also differed from the above sample in its single Aitken modal number distribution, peaking at 45 nm in diameter with a tail into the accumulation mode (Fig. 8, PI-8) causally related to its source in the free troposphere with likely marginal influence from marine sources. Ranging from 0.10 to 0.73 % water vapour, SS particles between 50 to 170 nm in diameter were activated (Fig. 7).

As shown in Fig. 11(PI-8), the SOL and AD_ext and PIN_ext assumptions gave the best overall fit to the observed CCNC, but only the PIN_ext case was able to reproduce the measured CCNC within 1 standard deviation for the whole SS range. It can be argued that the activated fractions of the broad Aitken mode encompassed an external mixture of particles with low water solubility that are highly surface active and internal mixtures of water soluble constituents.

Impactor sample MIZ-1: impactor sample MIZ-1 showed, similarly to the samples PI-1, PI-10 and PI-15, a bimodal aerosol number distribution with the Aitken and accumulation modes separated with a Hoppel minimum (Fig. 8, MIZ-1) but exhibited, similarly to PI-8, a more or less continuous increase in CCNC with increasing water vapour SS.

Based on the aerosol activation-limit dry diameters for MIZ-1 (Fig. 7), the range of all five water vapour SS (0.1 to 0.8 %) activated the particles in both the accumulation and Aitken modes down to ca. 50 nm in diameter.

As seen in Fig. 11 (MIZ-1), none of the simulated cases was able to reproduce the measured CCNC (within 1 standard deviation) over the entire SS range. For the lowest range of chosen water vapour SS the discrepancy is shown as an under-prediction of the observed CCNC, whereas quite the opposite is seen for SS above 0.2 %.

9 Modifying the condensation accommodation coefficient

A general conclusion to be drawn from the above simulations is the hydrophobic character of the collected aerosols, which in turn would impede water uptake with decreasing diameter of the aerosol. This was also indicated in the deviation from “ κ -theory” discussed in Sect. 5.

To further study this “hydrophobic” feature of the high Arctic aerosol we added two simulations based on the AD simulation but with a modified condensation accommodation coefficient, α_c . The condensation accommodation coefficient is a quantity characterizing the behaviour of the water molecules in their collisions with the aerosol surface. The value of α_c depends on the surface nature and state as well as on the water vapour SS pressure.

It has proved difficult to determine α_c experimentally. Davis (2006) reports on values varying by several orders of magnitude. For pure water and aqueous ionic solutions without surface covers several recent studies indicate that α_c is close to 1 (e.g. Winkler et al., 2004, 2006; Morita et al., 2004). However, several additional studies indicate that water vapour mass transport across the droplet–air interface in atmospheric aerosol may be limited, consistent with a lower value for α_c (e.g. Shantz et al., 2010; Ruehl et al., 2008; Chuang, 2003). Impeding water vapour mass transfer slows down the kinetics and this could result in the aerosol droplets not having sufficient time to grow to cloud droplet sizes in the CCN counter.

Consistent with the ambient measurements, laboratory studies by Abbatt et al. (2005) showed that thick covers of solid stearic acid were able to shut down the CCN ability of ammonium sulfate particles and the authors attributed this phenomenon to kinetic effects. Takahama and Russell (2011) found, using molecular dynamics simulations, that α_c of a partially covered water surface is roughly proportional to the fractional surface coverage. In this study, we tested two different surface coverage scenarios referred to as AC1 and AC2. The AC1 scenario had the same properties as the AD case, but with a constantly low $\alpha_c = 10^{-3}$. This would correspond to an almost completely covered aerosol droplet with unlimited resources of surface-covering molecules. AC2 shared properties with the AC1 assump-

tion except that it was assumed that the available surface covering agent is limited so that every particle has a constant absolute surface area covered. This can be expressed by $\alpha_c = 1 - (D_0/D)^2$ for $D > D_0$ and $\alpha_c = 0$ for $D \leq D_0$, where D is the wet particle diameter and D_0 is a reference diameter. This parameterization makes $\alpha_c = 0$ for small wet diameters and it asymptotically approaches unity for large wet diameters. Clearly, there are multiple other choices of parameterizations, which would serve as well, but the data available are not sufficient to distinguish between them. Neither is it possible to unambiguously determine a best value for D_0 . Hence, the AC1 and AC2 simulations should be viewed as tests of the idea that kinetic effects could reduce the CCN ability as suggested by Abbatt et al. (2005) and Takahama and Russell (2011). Table 4 lists the new assumptions concerning the “missing non-water soluble fraction” used in the AC1 and AC2 modelling. Black edges indicate surface covers impeding water vapour mass transport across the surface, yielding a lower condensation accommodation coefficient.

The simulation using the AC1 assumption under-predicted the observed CCNC within 1 standard deviation for the full range of water vapour SS studied and for all five impactor samples. These simulations are therefore not included in the compilation of the impactor samples shown in Fig. 12. The result of the AC2 sceneries will be discussed below.

The AC2 simulation of sample PI-1 was able to capture the sensitivity of the measured CCNC within 1 standard deviation as a function of all five levels of water vapour SS ranging from 0.1 to 0.6%. This argues for the type 10 d, e particles, with a limited water vapour mass transport across the droplet–air interface, coexisting with the type 10a–c particles at the large-end tail of the Aitken mode. For impactor sample PI-15 the AC2 CCNC simulation as a function of all five levels of water vapour SS showed similarly success (Fig. 12, PI-15). In Sect. 8 above it was argued that the activated fractions of the accumulation mode particles (PI-15) encompassed an external mixture of partly wetted gel-type particles with their shown hydrophobic character and impenitent water vapour uptake (being more dominant with decreasing diameter) with internal mixtures of water-soluble constituents strong in DMS-derived sulfur. Also for sample PI-10 (Fig. 11) this feature of a limited water vapour mass transport across the droplet–air interface of the accumulation mode seems to be the best possible explanation of the over-prediction of CCNC seen for water vapour SS above 0.2% for PI-10.

It was argued based on the simulations shown in Fig. 11 (PI-8) that the activated fraction of the Aitken mode of impactor sample PI-8 encompassed an external mixture of particles with low water solubility that are highly surface active and with internal mixtures of water soluble constituents. The simulations with modified condensation accommodation coefficients, however, strongly under-predicted the observed CCNC at the higher SSs; see Fig. 12 (PI-8). Therefore, we

did not find any evidence for a restricted water uptake in this sample.

The simulations performed for sample MIZ-1 in Sect. 8 were not at all successful in reproducing the measured CCNC within 1 standard deviation for the entire SS range (broadly activated particles in both the accumulation and Aitken modes down to ca. 50 nm in diameter): the lowest range of water vapour SS showed an under-prediction of the observed CCNC whereas an over-prediction was seen for SS above 0.2%. With the added assumption in the AC2 simulation it was still hard to capture the overall continued increase in observed CCNC with increasing water vapour SS pressures.

We note further that by lowering the D_0 in the AC2 simulation (physically that is equivalent to increasing the available surface coverage area), it seems possible to get a better match. However, we consider this as curve fitting beyond the scope and available data of this study.

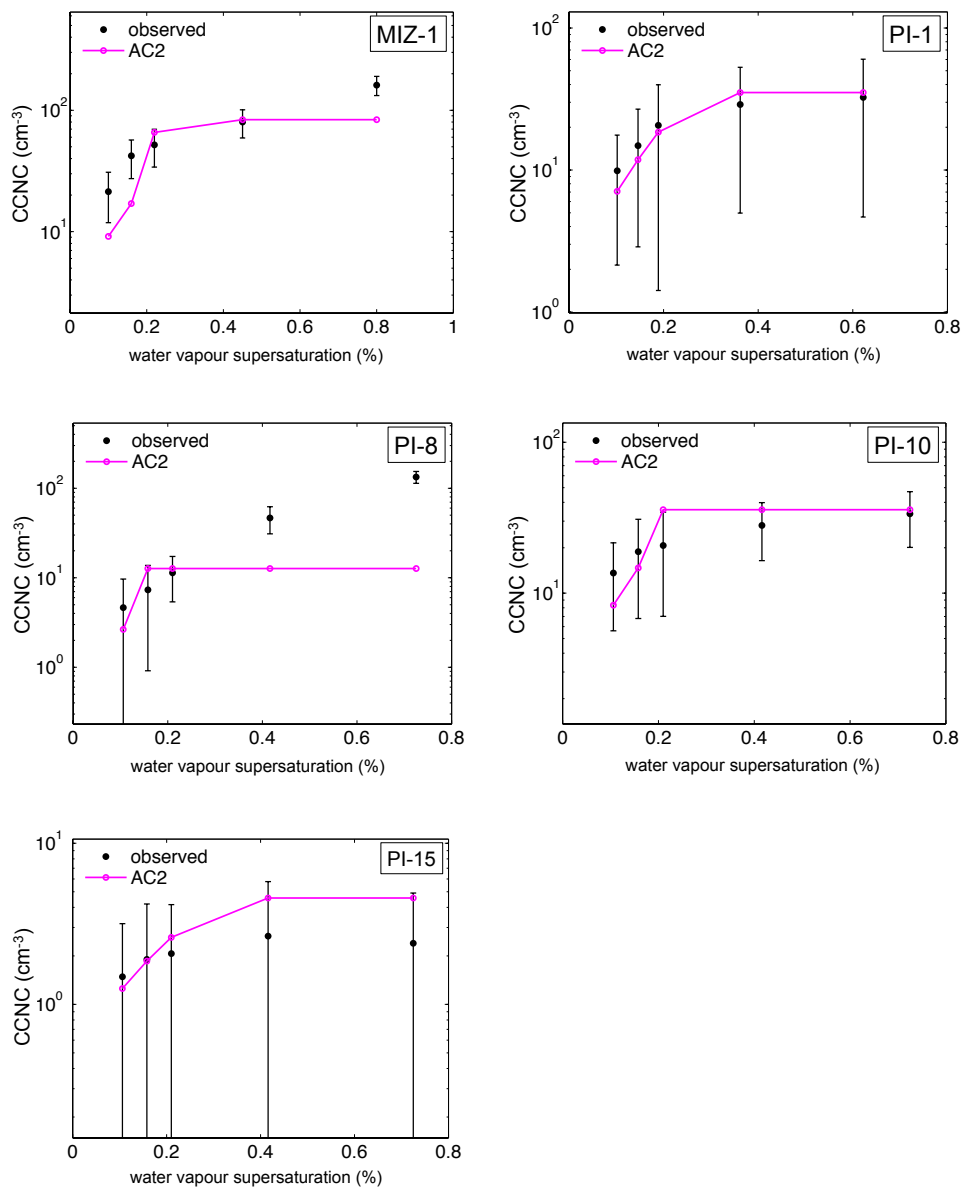
10 Summary and conclusions

Concentrations of cloud condensation nuclei were measured throughout an icebreaker expedition (ASCOS) over the central Arctic Ocean, including a 3 week ice drift operation at 87° N, from 3 August to 9 September 2008. Median daily CCNC typically ranged from 15 to 30 cm⁻³, being a factor of three higher at the MIZ. The most conspicuous feature of the time series of CCN was the 2–3 orders of magnitude range of concentrations, from below 1 to 100 cm⁻³. Highest concentrations occurred over the open water just south of the ice edge in August. Losses of CCN as the air progressed over the pack ice and mixing processes in an often strongly stratified near-surface layer were suggested to contribute most strongly to this large range (Bigg et al., 2001). The losses of CCN (measured at 0.2% SS) approaching a factor of 3 during the first ca. 2 days in air progressing from the open sea to the pack ice were not surprising in view of the usual evolution of cloudiness that accompanies the progression into the pack ice. It was surprising however that the losses did not continue for longer transport times. A local surface source, presumed to be the bursting of bubbles on the surface of open leads, was suggested, consistent with previous independent analyses (e.g. Leck and Bigg, 2005a). This open lead source of particles has recently been demonstrated to be biogenic and to consist of marine polymer gels (Orellana et al., 2001; Leck et al., 2012).

In previous searches for a relationship between the properties of the summer high Arctic aerosol and its ability to form CCN by assuming equilibrium Köhler theory or conventional κ -Köhler theory (Zhou et al., 2001; Bigg and Leck, 2001a; Martin et al., 2011) the calculations generally tended to over-predict the observed CCNC. The prediction was about 30–60% higher than the observed values for water vapour SS above 0.4% (Martin et al., 2011). Below 0.2% water vapour SS in general an excellent agreement was achieved. Further,

Table 4. Assumptions on the missing non-water soluble aerosol fraction used in the simulations, with modified condensation accommodation coefficients.

Simulation	Illustration	Description
AC1		As the AD case, but with the condensation accommodation coefficient set to 10^{-4} .
AC2		As the AD case, but with a variable condensation accommodation coefficient, see text for details.

**Figure 12.** Observed and simulated CCNC for samples MIZ-1, PI-1, PI-8, PI-10 and PI-15, ranging from 0.1 to 0.8% water vapour SS. Error bars represent 1 standard deviation. AC2 correspond to the assumption AD (see Table 2), with a variable condensation accommodation coefficient.

Lohmann and Leck (2005) found it necessary to invoke a highly externally mixed surface-active Aitken mode in order to explain the observed CCNC over the pack ice.

The authors being intrigued by the above results, the present study was aimed to further reduce some of the uncertainties surrounding the CCN properties promoting/suppressing cloud droplet formation in a marine environment with limited influences from man-made activities. The main advantage and motivation compared to previous high Arctic CCN-closure studies was the use of water soluble aerosol bulk chemistry obtained from highly size resolved impactor samples. This enabled us also to make a similarly highly size resolved best “guess” of the unexplained number fraction assumed to be organic in nature. Guided by chemical analyses based on electron microscope data from all three previous expeditions (Bigg and Leck, 2001a, 2001b, 2008; Leck and Bigg, 1999, 2002, 2005a, 2005b, 2010; Leck et al., 2002; Lohman and Leck, 2005), we used various water soluble, slightly water soluble and non-water soluble proxy constituents. One further advantage was the possibility to compare the measured and modelled CCNC for more than one set level of water vapour SS, ranging from 0.1 to 0.8%. The simulations assumed equilibrium Köhler theory and were based on the diffusional growth equation. In addition, calculations were performed using κ -Köhler theory.

The results of this study are consistent with previous results by Martin et al. (2011) in that conventional κ -Köhler theory fails to predict the CCNC for samples in air that had been advected over the pack ice. Simulating the cloud nucleation process using a Lagrangian adiabatic air parcel model that solves the kinetic formulation for condensation of water on size resolved aerosol particles at high SS resulted in severe over-predictions of the CCNC when even the most conservative assumption on the unknown fraction was used. A general conclusion to be drawn from the CCN simulations and from the calculated deviation from κ -Köhler theory is an increase of the hydrophobic character in the activated particles with decreasing diameter. This suggested hydrophobic character of the high Arctic aerosol was also shown in the study of Martin et al. (2011) and would in turn impede water uptake with decreasing diameter of the aerosol.

We tested whether introducing kinetic limitations on water uptake could explain these aerosol properties suppressing cloud droplet activation above 0.4% water vapour SS. A fixed non-size resolved low water uptake rate consistently produced too low CCNC, but a size-dependent assumptions was in general able to capture the sensitivity of the measured CCNC within 1 standard deviation as a function of all the five levels of water vapour SS ranging from 0.1 to 0.8%.

The results further suggested that either differences in time of advection of the air over the pack ice, where additional primary marine aerosol sources and atmospheric gas-phase and aerosol dynamical processes could change the properties of the CCN prior to collection, or possible impact from non-natural aerosol sources did have systematic effects on the

sensitivity of observed CCNC as a function of water vapour SS. What seems to be of primary importance is the size resolved state of mixture together with physical and chemical behaviour of the fraction of the aerosol population that will undergo droplet activation.

To explain the results we propose that the portion of the internally/externally mixed water insoluble particles, which were physically and chemically behaving as polymer gels, was larger in the corresponding smaller aerosol sizes ranges. The suggestion of the presence of a non-water soluble organic fraction of the CCN population either promoting or suppressing cloud droplet formation thus did not deviate from the conclusions drawn by Lohman and Leck (2005) and Martin et al. (2011). The interaction of the hydrophilic and hydrophobic entities on the structures of polymer gels during cloud droplet activation strongly suggests a dichotomous behaviour with at first only partial wetting character and only weak hygroscopic growth. Given time, a high CCN activation efficiency is achieved, which is promoted by the hydrophilicity or surface-active properties of the gels (Ovadnevaite et al., 2011). The results of this study argue for the behaviour of the high Arctic aerosol in CCN counters operating at high relative humidities being not fully explained by conventional Köhler theory, where the only free parameters are hygroscopicity and surface tension. However, we note that particles with kinetically restricted growth can be activated in real cloud situations even if they are not counted in the CCN counter. It might be that the time (~ 50 s) inside the CCN counter is insufficient for the particles to grow to large enough sizes. The results of Chuang (2003) show consistency with the findings in this study in that he found that an externally mixed fraction of ambient aerosol, with very slow water uptake, could account for some observations of particle water uptake that could not be explained with conventional Köhler theory.

Clearly, many uncertainties remain in the evolution of cloud-active particles in the high Arctic and probably elsewhere. One evident outcome from this study is that we have to stop regarding the cloud-active particles over remote marine areas as simply inorganic soluble salts, and regard them in addition as consisting of internal/external mixtures of soluble or slightly soluble organics, which likely will influence the equilibrium water vapour pressure and decrease surface tension of the droplets to be formed. This study also suggests that the Köhler equation used for simulating cloud droplet activation is not sufficient for describing the condensational growth of the interaction of the hydrophilic and hydrophobic entities on the structures of the polymer gels suggested to be present at the MIZ and over the pack ice area. Different approaches are suggested as revisions of Köhler theory, one being to utilize a larger number of size resolved observations of morphology, state of mixture and chemical and physical behaviour of individual cloud-active particles.

The Supplement related to this article is available online at doi:10.5194/acp-15-2545-2015-supplement.

Acknowledgements. We greatly thank Maria Martin, Staffan Sjöberg, Douglas Orsini, Berko Sierau, Ulrike Lohmann, Erik Swietlicki and Jost Heintzenberg for the CCN and aerosol physical data collection and quality assurance work. Jost Heintzenberg's comments on the paper are appreciated. This work is part of ASCOS (the Arctic Summer Cloud Ocean Study). ASCOS was made possible by funding from the Knut and Alice Wallenberg Foundation and the DAMOCLES European Union 6th Framework Program Integrated Research Project. The Swedish Polar Research Secretariat (SPRS) provided access to the icebreaker *Oden* and logistical support. Michael Tjernström is specifically thanked for his co-coordination of ASCOS. We are grateful to the SPRS logistical staff and to *Oden's* Captain Mattias Peterson and his crew. ASCOS is an IPY project under the AICIA-IPY umbrella and an endorsed SOLAS project. The Swedish Research Council (VR), the Knut and Alice Wallenberg Foundation and the Bolin Centre for Climate Research at Stockholm University provided support for this work.

Edited by: J. W. Bottenheim

References

- Abbatt, J. P. D., Broekhuizen, K., and Pradeep Kumar, P.: Cloud condensation nucleus activity of internally mixed ammonium sulfate/organic acid aerosol particles, *Atmos. Environ.*, 39, 4767–4778, 2005.
- Bigg, E. K. and Leck, C.: Cloud-active particles over the central Arctic Ocean, *J. Geophys. Res.*, 106, 32155–32166, 2001a.
- Bigg, E. K. and Leck, C.: Properties of the aerosol over the central Arctic Ocean, *J. Geophys. Res.*, 106, 32101–32109, 2001b.
- Bigg, E. K. and Leck, C.: The composition of fragments of bubbles bursting at the ocean surface, *J. Geophys. Res.*, 113, 1209, doi:10.1029/2007JD009078, 2008.
- Bigg, E. K., Leck, C., and Nilsson, E. D.: Sudden changes in arctic atmospheric aerosol concentrations during summer and autumn, *Tellus*, 48B, 254–271, 1996.
- Bigg, E. K., Leck, C., and Nilsson, E. D.: Sudden changes in aerosol and gas concentrations in the central Arctic marine boundary layer: Causes and consequences, *J. Geophys. Res.*, 106, 32167–32185, 2001.
- Birmili, W., Stratmann, F., and Wiedensohler, A.: Design of a DMA-based size spectrometer for a large particle size range and stable operation, *J. Aerosol Sci.*, 30, 549–553, 1999.
- Chang, R. Y.-W., Leck, C., Graus, M., Müller, M., Paatero, J., Burkhardt, J. F., Stohl, A., Orr, L. H., Hayden, K., Li, S.-M., Hansel, A., Tjernström, M., Leaitch, W. R., and Abbatt, J. P. D.: Aerosol composition and sources in the central Arctic Ocean during ASCOS, *Atmos. Chem. Phys.*, 11, 10619–10636, doi:10.5194/acp-11-10619-2011, 2011.
- Chuang, P.: Measurement of the timescale of hygroscopic growth for atmospheric aerosols, *J. Geophys. Res.*, 108, 4282, doi:10.1029/2002JD002757, 2003.
- Davis, E. J.: A history and state-of-the-art of accommodation coefficients, *Atmos. Res.*, 82, 561–578, 2006.
- Draxler, R. R. and Rolph, G. D.: HYSPLIT (HYbrid Single-Particle Lagrangian Integrated Trajectory) Model access via NOAA ARL READY Website, available at: <http://ready.arl.noaa.gov/HYSPLIT.php> (last access: 7 April 2010), NOAA Air Resources Laboratory, Silver Spring, MD, 2011.
- EANET (Acid Deposition Monitoring Network in East Asia): Report of the Inter-Laboratory Comparison Project 2007, available at: <http://www.eanet.asia/product/>, 2008.
- Engvall, A.-C., Krejci, R., Ström, J., Treffeisen, R., Scheele, R., Hermansen, O., and Paatero, J.: Changes in aerosol properties during spring-summer period in the Arctic troposphere, *Atmos. Chem. Phys.*, 8, 445–462, doi:10.5194/acp-8-445-2008, 2008.
- Fu, P., Kawamura, K., Chen, J., and Barrie, L. A.: Isoprene, Monoterpene, and Sesquiterpene Oxidation Products in the High Arctic Aerosols during Late Winter to Early Summer, *Environ. Sci. Technol.*, 43, 4022–4028, 2009.
- Gao, Q., Leck, C., Rauschenberg, C., and Matrai, P. A.: On the chemical dynamics of extracellular polysaccharides in the high Arctic surface microlayer, *Ocean Sci.*, 8, 401–418, doi:10.5194/os-8-401-2012, 2012.
- Hamacher-Barth, E., Jansson, K., and Leck, C.: A method for sizing submicrometer particles in air collected on Formvar films and imaged by scanning electron microscope, *Atmos. Meas. Tech.*, 6, 3459–3475, doi:10.5194/amt-6-3459-2013, 2013.
- Hede, T., Li, X., Leck, C., Tu, Y., and Ågren, H.: Model HULIS compounds in nanoaerosol clusters – investigations of surface tension and aggregate formation using molecular dynamics simulations, *Atmos. Chem. Phys.*, 11, 6549–6557, doi:10.5194/acp-11-6549-2011, 2011.
- Heintzenberg, J. and Leck, C.: The summer aerosol in the central Arctic 1991–2008: did it change or not?, *Atmos. Chem. Phys.*, 12, 3969–3983, doi:10.5194/acp-12-3969-2012, 2012.
- Heintzenberg, J., Birmili, W., Wiedensohler, A., Nowak, A., and Tuch, T.: Structure, variability and persistence of the submicrometer marine aerosol, *Tellus*, 56B, 4, 357–367, 2004.
- Herman, G. and Goody, R.: Formation and persistence of summertime Arctic stratus clouds, *J. Atmos. Sci.*, 33, 1537–1553, 1976.
- Hinds, W. C.: *Aerosol Technology: Properties, Behavior, and Measurement of Airborne Particles*, Wiley-Interscience, 504 pp., ISBN: 978-0-471-19410-1, 1999.
- Hoppel, W. A., Frick, G. M., and Larson, R. E.: Effect of non-precipitating clouds on the aerosol size distribution in the marine boundary layer, *Geophys. Res. Lett.*, 13, 125–128, 1986.
- Hoppel, W. A., Frick, G. M., Fitzgerald, J. W., and Larson, R. E.: Marine boundary layer measurements of new particle formation and the effects non precipitating clouds have on aerosol size distribution, *J. Geophys. Res.*, 99, 14443–14459, doi:10.1029/94JD00797, 1994.
- Intrieri, J. M., Fairall, C. W., Shupe, M. D., Persson, P. O. G., Andreas, E. L., Guest, P. S., and Moritz, R. E.: An annual cycle of Arctic surface cloud forcing at SHEBA, *J. Geophys. Res.*, 107, 8039, doi:10.1029/2000JC000439, 2002.
- Karl, M., Gross, A., Leck, C., and Pirjola, L.: Intercomparison of dimethylsulfide oxidation mechanisms for the marine boundary layer: Gaseous and particulate sulfur constituents, *J. Geophys. Res.-Atmos.*, 112, D15304, 2007.

- Karl, M., Leck, C., Gross, A., and Pirjola, L.: A study of new particle formation in the marine boundary layer over the central Arctic Ocean using a flexible multicomponent aerosol dynamic model, *Tellus B*, 64, 17158, doi:10.3402/tellusb.v64i0.17158, 2012.
- Karl, M., Leck, C., Coz, E., and Heintzenberg, J.: Marine nanogels as a source of atmospheric nanoparticles in the high Arctic, *Geophys. Res. Lett.*, 40, 3738–3743, doi:10.1002/grl.50661, 2013.
- Kay, J. E. and Gettelman, A.: Cloud influence on and response to seasonal Arctic sea ice loss, *J. Geophys. Res.*, 114, D18204, doi:10.1029/2009JD011773, 2009.
- Kerminen, V.-M. and Leck, C.: Sulfur chemistry over the central Arctic Ocean during the summer: Gas-to-particle transformation, *J. Geophys. Res.*, 106, 32087–32099, 2001.
- Kupiszewski, P., Leck, C., Tjernström, M., Sjogren, S., Sedlar, J., Graus, M., Müller, M., Brooks, B., Swietlicki, E., Norris, S., and Hansel, A.: Vertical profiling of aerosol particles and trace gases over the central Arctic Ocean during summer, *Atmos. Chem. Phys.*, 13, 12405–12431, doi:10.5194/acp-13-12405-2013, 2013.
- Köhler, H.: The nucleus in and the growth of hygroscopic droplets, *T. Faraday Soc.*, 32, 1152–1161, 1936.
- Lannefors, H., Heintzenberg, J., and Hansson, H.-C.: A comprehensive study of physical and chemical parameters of the Arctic summer aerosol; results from the Swedish expedition Ymer-80, *Tellus*, 35B, 40–54, 1983.
- Leaich, W. R., Strapp, J. W., and Isaac, G. A.: Cloud droplet nucleation and cloud scavenging of aerosol sulfate in polluted atmospheres, *Tellus*, 38B, 328–344, 1986.
- Leck, C. and Bigg, E. K.: Aerosol production over remote marine areas – A new route, *Geophys. Res. Lett.*, 23, 3577–3581, 1999.
- Leck, C. and Bigg, E. K.: Biogenic particles in the surface microlayer and overlying atmosphere in the central Arctic Ocean during summer, *Tellus*, 57B, 305–316, 2005a.
- Leck, C. and Bigg, E. K.: Evolution of the marine aerosol – A new perspective. *Geophys. Res. Lett.*, 32, L19803, doi:10.1029/2005GL023651, 2005b.
- Leck, C. and Bigg, E. K.: New particle formation of marine biological origin, *Aerosol Sci. Tech.*, 44, 570–577, 2010.
- Leck, C. and Persson, C.: Seasonal and short-term variability in dimethyl sulfide, sulfur dioxide and biogenic sulfur and sea salt aerosol particles in the arctic marine boundary layer, during summer and autumn, *Tellus*, 48B, 272–299, 1996.
- Leck, C., Bigg, E. K., Covert, D. S., Heintzenberg, J., Maenhaut, W., Nilsson, E. D., and Wiedensohler, A.: Overview of the atmospheric research program during the International Arctic Ocean Expedition of 1991 (IAOE-91) and its scientific results, *Tellus*, 48B, 136–155, 1996.
- Leck, C., Nilsson, E. D., Bigg, E. K., and Bäcklin, L.: Atmospheric program on the Arctic Ocean Expedition 1996 (AOE-96): an overview of scientific goals, experimental approaches, and instruments, *J. Geophys. Res.*, 106, 32051–32067, 2001.
- Leck, C., Norman, M., Bigg, E. K., and Hillamo, R.: Chemical composition and sources of the high Arctic aerosol relevant for cloud formation, *J. Geophys. Res.*, 107, 4135, doi:10.1029/2001JD001463, 2002.
- Leck, C., Tjernström, M., Matrai, P., Swietlicki, E., and Bigg, K.: Can marine micro-organisms influence melting of the Arctic pack ice?, *EOS T. Am. Geophys. Un.*, 85, 25–32, doi:10.1029/2004EO030001, 2004.
- Leck, C., Gao, Q., Mashayekhy Rad, F., and Nilsson, U.: Size resolved airborne particulate polysaccharides in summer high Arctic, *Atmos. Chem. Phys. Discuss.*, 13, 9801–9847, doi:10.5194/acpd-13-9801-2013, 2013.
- Lelieveld, J. and Heintzenberg, J.: Sulfate cooling effect on climate through in-cloud oxidation of anthropogenic SO₂, *Science*, 258, 117–120, 1992.
- Lohmann, U. and Leck, C.: Importance of submicron surface-active organic aerosols for pristine Arctic clouds, *Tellus*, 57B, 261–268, 2005.
- Martin, M., Chang, R. Y.-W., Sierau, B., Sjogren, S., Swietlicki, E., Abbatt, J. P. D., Leck, C., and Lohmann, U.: Cloud condensation nuclei closure study on summer arctic aerosol, *Atmos. Chem. Phys.*, 11, 11335–11350, doi:10.5194/acp-11-11335-2011, 2011.
- Mauritsen, T., Sedlar, J., Tjernström, M., Leck, C., Martin, M., Shupe, M., Sjogren, S., Sierau, B., Persson, P. O. G., Brooks, I. M., and Swietlicki, E.: An Arctic CCN-limited cloud-aerosol regime, *Atmos. Chem. Phys.*, 11, 165–173, doi:10.5194/acp-11-165-2011, 2011.
- Morita, A., Sugiyama, M., Kameda, H., Koda, S., and Hanson, D. R.: Mass Accommodation Coefficient of Water: Molecular Dynamics Simulation and Revised Analysis of Droplet Train/Flow Reactor Experiment, *J. Phys. Chem. B.*, 108, 9111–9120, 2004.
- Narukawa, M., Kawamura, K., Li, S.-M., and Bottenheim, J. W.: Dicarboxylic acids in the Arctic aerosols and snowpacks collected during ALERT 2000, *Atmos. Environ.*, 36, 2491–2499, 2002.
- Nilsson, E. D.: Planetary boundary layer structure and air mass transport during the International Arctic Ocean Expedition 1991, *Tellus*, 48B, 178–196, 1996.
- Nilsson, E. D., Rannik, Ü., Swietlicki, E., Leck, C., Aalto, P. P., Norman, M., and Zhou, J.: Turbulent aerosol number fluxes during the Arctic Ocean Expedition 1996, part II: a wind driven source of sub micrometers aerosol particles from the sea, *J. Geophys. Res.*, 106, 32139–32154, 2001.
- Norris, S. J., Brooks, I. M., de Leeuw, G., Sirevaag, A., Leck, C., Brooks, B. J., Birch, C. E., and Tjernström, M.: Measurements of bubble size spectra within leads in the Arctic summer pack ice, *Ocean Sci.*, 7, 129–139, doi:10.5194/os-7-129-2011, 2011.
- Ovadnevaite, J., Ceburnis, D., Martucci, G., Bialek, J., Monahan, C., Rinaldi, M., Facchini, M. C., Berresheim, H., Worsnop, D. R., and O’Dowd, C.: Primary marine organic aerosol: A dichotomy of low hygroscopicity and high CCN activity, *Geophys. Res. Lett.*, 38, L21806, doi:10.1029/2011GL048869, 2011.
- Orellana, M. V., Matrai, P. A., Leck, C., Rauschenberg, C. D., Lee, A. M., and Coz, E.: Marine microgels as a source of cloud condensation nuclei in the high Arctic, *P. Natl. Acad. Sci.*, 108, 13612–13617, 2011.
- Paatero, J., Vaattovaara, P., Vestenius, M., Meinander, O., Makkonen, U., Kivi, R., Hyvärinen, A., Asmi, E., Tjernström, M., and Leck, C.: Finnish contribution to the Arctic Summer Cloud Ocean Study (ASCOS) expedition, Arctic Ocean 2008, *Geophysica*, 45, 119–146, 2009.
- Petters, M. D. and Kreidenweis, S. M.: A single parameter representation of hygroscopic growth and cloud condensation nucleus activity, *Atmos. Chem. Phys.*, 7, 1961–1971, doi:10.5194/acp-7-1961-2007, 2007.
- Pruppacher, H. R. and Klett, J. D.: *Microphysics of Clouds and Precipitation*, Kluwer Academic Publishers, Dordrecht, 1997.

- Roberts, G. C. and Nenes, A.: A continuous-flow stream wise thermal-gradient CCN chamber for atmospheric measurements, *Aerosol Sci. Technol.*, 39, 206–221, doi:10.1080/027868290913988, 2005.
- Rolph, G.D.: Real-time Environmental Applications and Display sYstem (READY) available at: (<http://ready.arl.noaa.gov>). NOAA Air Resources Laboratory, Silver Spring, MD., 2011. Air Resources Laboratory, Silver Spring, MD., 2011.
- Ruehl, C. R., Chuang, P. Y., and Nenes, A.: How quickly do cloud droplets form on atmospheric particles?, *Atmos. Chem. Phys.*, 8, 1043–1055, doi:10.5194/acp-8-1043-2008, 2008.
- Sedlar, J., Tjernström, M., Mauritsen, T., Shupe, M. D., Brooks, I. M., Persson, P. O. G., Birch, C. E., Leck, C., Sirevaag, A., and Nicolaus, M.: A transitioning Arctic surface energy budget: the impacts of solar zenith angle, surface albedo and cloud radiative forcing, *Clim. Dynam.*, 37, 1643–1660, doi:10.1007/s00382-010-0937-5, 2011.
- Shantz, N. C., Chang, R. Y.-W., Slowik, J. G., Vlasenko, A., Abbatt, J. P. D., and Leaitch, W. R.: Slower CCN growth kinetics of anthropogenic aerosol compared to biogenic aerosol observed at a rural site, *Atmos. Chem. Phys.*, 10, 299–312, doi:10.5194/acp-10-299-2010, 2010.
- Shupe, M. D., Persson, P. O. G., Brooks, I. M., Tjernström, M., Sedlar, J., Mauritsen, T., Sjogren, S., and Leck, C.: Cloud and boundary layer interactions over the Arctic sea ice in late summer, *Atmos. Chem. Phys.*, 13, 9379–9399, doi:10.5194/acp-13-9379-2013, 2013.
- Sierau, B., Chang, R. Y.-W., Leck, C., Paatero, J., and Lohmann, U.: Single-particle characterization of the high-Arctic summertime aerosol, *Atmos. Chem. Phys.*, 14, 7409–7430, doi:10.5194/acp-14-7409-2014, 2014.
- Svenningsson, B., Rissler, J., Swietlicki, E., Mircea, M., Bilde, M., Facchini, M. C., Decesari, S., Fuzzi, S., Zhou, J., Mønster, J., and Rosenørn, T.: Hygroscopic growth and critical supersaturations for mixed aerosol particles of inorganic and organic compounds of atmospheric relevance, *Atmos. Chem. Phys.*, 6, 1937–1952, doi:10.5194/acp-6-1937-2006, 2006.
- Takahama, S. and Russell, L. M.: A molecular dynamics study of water mass accommodation on condensed phase water coated by fatty acid monolayers, *J. Geophys. Res.*, 116, D02203, doi:10.1029/2010JD014842, 2011.
- Tang, I. N. and Munkelwitz, H. R.: Water activities, densities, and refractive indices of aqueous sulfates and sodium nitrate droplets of atmospheric importance, *J. Geophys. Res.*, 99, 18 801–18 808, 1994.
- Tjernström, M., Leck, C., Persson, P. O., Jensen, M., Oncley, S., and Targino, A.: The Summertime Arctic Atmosphere: Meteorological measurements during the Arctic Ocean Experiment 2001 (AOE-2001), *B. Am. Meteorol. Soc.*, 85, 1305–1321, 2004.
- Tjernström, M., Sedlar, J., and Shupe, M. D.: How well do regional climate models reproduce radiation and clouds in the Arctic?, *J. Appl. Meteorol. Clim.*, 47, 2405–2422, 2008.
- Tjernström, M., Birch, C. E., Brooks, I. M., Shupe, M. D., Persson, P. O. G., Sedlar, J., Mauritsen, T., Leck, C., Paatero, J., Szczodrak, M., and Wheeler, C. R.: Meteorological conditions in the central Arctic summer during the Arctic Summer Cloud Ocean Study (ASCOS), *Atmos. Chem. Phys.*, 12, 6863–6889, doi:10.5194/acp-12-6863-2012, 2012.
- Tjernström, M., Leck, C., Birch, C. E., Bottenheim, J. W., Brooks, B. J., Brooks, I. M., Bäcklin, L., Chang, R. Y.-W., de Leeuw, G., Di Liberto, L., de la Rosa, S., Granath, E., Graus, M., Hansel, A., Heintzenberg, J., Held, A., Hind, A., Johnston, P., Knulst, J., Martin, M., Matrai, P. A., Mauritsen, T., Müller, M., Norris, S. J., Orellana, M. V., Orsini, D. A., Paatero, J., Persson, P. O. G., Gao, Q., Rauschenberg, C., Ristovski, Z., Sedlar, J., Shupe, M. D., Sierau, B., Sirevaag, A., Sjogren, S., Stetzer, O., Swietlicki, E., Szczodrak, M., Vaattovaara, P., Wahlberg, N., Westberg, M., and Wheeler, C. R.: The Arctic Summer Cloud Ocean Study (ASCOS): overview and experimental design, *Atmos. Chem. Phys.*, 14, 2823–2869, doi:10.5194/acp-14-2823-2014, 2014.
- Tuckermann, R.: Surface tension of aqueous solutions of water-soluble organic and inorganic compounds, *Atmos. Environ.*, 41, 6265–6275, 2007.
- Twomey, S.: Pollution and the planetary albedo, *Atmos. Environ.*, 8, 1251–1256, 1974.
- Verdugo, P.: Marine Microgels, *Ann. Rev. Marine Sci.*, 4, 375–400, doi:10.1146/annurev-marine-120709-142759, 2012.
- Walsh, J., Kattsov, V., Chapman, W., Govorkova, V., and Pavlova, T.: Comparison of Arctic climate simulations by uncoupled and coupled global models, *J. Climate*, 15, 1429–1446, 2002.
- Winkler, P. M., Vrtala A., Wagner, P. E., Kulmala, M., Lehtinen, K. E. J., and Vesala, T.: Mass and Thermal Accommodation during Gas-Liquid Condensation of Water, *Phys. Rev. Lett.*, 93, 075701, doi:10.1103/PhysRevLett.93.075701, 2004.
- Winkler, P. M., Vrtala, A., Rudolf, R., Wagner, P. E., Riipinen, I., Vesala, T., Lehtinen, K. E. J., Viisanen, Y., and Kulmala, M.: Condensation of water vapor: Experimental determination of mass and thermal accommodation coefficients, *J. Geophys. Res.*, 111, D19202, doi:10.1029/2006JD007194, 2006.
- Xin L., Leck, C., Sun, L., Hede, T., Tu, Y., and Ågren, H.: Cross-Linked Polysaccharide Assemblies in Marine Gels: An Atomistic Simulation, *J. Phys. Chem. Lett.*, 4, 2637–2642, doi:10.1021/jz401276r, 2013.
- Zhou, J., Swietlicki, E., Berg, O. H., Aalto, P. P., Hämeri, K., Nilsson E. D., and Leck, C.: Hygroscopic properties of aerosol particles over the central Arctic Ocean during summer, *J. Geophys. Res.*, 106, 32111–32123, 2001.